Journal of the Mechanics and Physics of Solids 59 (2011) 1752–1776

Contents lists available at ScienceDirect

Journal of the Mechanics and Physics of Solids

journal homepage: www.elsevier.com/locate/jmps

A non-local visco-elastic damage model and dynamic fracturing

Vladimir Lyakhovsky [a,*], Yariv Hamiel [a], Yehuda Ben-Zion [b]

[a] Geological Survey of Israel, Jerusalem 95501, Israel
[b] Department of Earth Sciences, University of Southern California, Los Angeles, CA 90089-0740, USA

ARTICLE INFO

Article history:
Received 24 September 2010
Received in revised form
14 April 2011
Accepted 28 May 2011
Available online 6 June 2011

Keywords:
Fracture
Phase transformation
Dynamics
Constitutive Behavior
Damage rheology

ABSTRACT

We present an extended formulation of a non-linear continuum visco-elastic damage rheology that accounts for non-local damage accumulation, dynamic fracturing, and transition from solid to granular state in the slip zone. Generalizing the standard Hookean strain energy, the model has three additional energy terms: a non-analytic second-order function of the first and second strain invariants, a term proportional to the strain rate, and a term proportional to the spatial gradient of a damage state variable. The first term leads to non-linear stress–strain relation, with abrupt changes in the effective elastic moduli upon stress reversal from compression to tension along with damage- and stress-induced anisotropy. The second term gives rise to Kelvin–Voigt viscous relaxation. The resulting formulation combines Kelvin–Voigt and Maxwell visco-elasticity, accounting for both long-term relaxation and short-term dissipation stabilizing the damage evolution. The third term produces a finite length scale for damage diffusion that eliminates the unrealistic singular localization of the local damage model. An equation for damage evolution derived from basic thermodynamic considerations quantifies the kinetics of damage under different conditions, including quasi-static and dynamic degradation and gradual healing. In the vicinity of macroscopic failure, at a critical level of damage associated with loss of convexity of the energy function, the formulation includes a transition from damaged solid to granular flow dynamics. The formulation provides a framework for studying multiple aspects of brittle deformation, including potential feedback mechanisms between evolving elastic and related properties of the slip localization zone and subsequent rupture behavior. Several features of the model including existence of finite localization width and transition from slow to rapid dynamic slip are illustrated using numerical simulations. The analysis clarifies the dependency of some damage parameters on basic properties of the examined domain and boundary conditions, and the conditions for which simpler local damage descriptions are appropriate.

1. Introduction

Laboratory investigations indicate that fracturing of rocks and other brittle materials cannot generally be described in terms of single crack propagation in the framework of linear elastic fracture mechanics (e.g., Yukutake, 1989; Lockner et al., 1992; Nemat-Nasser and Hori, 1999; Paterson and Wong, 2005). The size and geometry of a region with intense distributed cracking, referred to as damage zone or process zone, control the trajectory and growth rate of quasi-static

* Corresponding author. Tel.: +972 2 5314265; fax: +972 2 5380688.
E-mail addresses: vladi@geos.gsi.gov.il (V. Lyakhovsky), yariv@gsi.gov.il (Y. Hamiel), benzion@usc.edu (Y. Ben-Zion).

0022-5096/$ - see front matter © 2011 Elsevier Ltd. All rights reserved.
doi:10.1016/j.jmps.2011.05.016

macro-cracks (e.g., Bazant and Cedolin, 1991; Zietlow and Labuz, 1998). Experimental analyses of acoustic emission (AE) during tri-axial loading tests demonstrate different stages of the intensity and spatial distributions of internal fractures (e.g., Lockner et al., 1992; Zang et al., 2000). At relatively low stresses, AE and fracturing occur over most of the sample. At relatively high stresses just before the peak stress, AE is localized in a relatively narrow damage zone. Finally, dynamic fracturing occurs along a narrow fault zone. These laboratory studies highlight the importance of accounting for the distribution of damage evolution in analysis of rock fracturing.

Damage rheology models have been applied extensively to model fracturing processes in engineering materials and rocks (e.g., Kachanov, 1986; Rabotnov, 1988; Krajcinovic, 1996; Lemaitre, 1996; Allix and Hild, 2002). Micromechanical damage models based on sets of micro-cracks satisfying each linear elastic fracture mechanics (e.g., Ashby and Sammis, 1990; Nemat-Nasser and Hori, 1999; Deshpande and Evans, 2008) provide physically based description of material damage. However, their application for constitutive laws and damage behavior of rocks is limited since most of the models are formulated based on deformation and growth of non-interacting penny-shaped micro-cracks. These simplifications may induce deviations from the actual state and evolution of damage especially close to failure at high microcrack concentrations. Continuum damage frameworks attempt to model the effective macroscopic properties associated with large populations of internal flaws without prescribing the micromechanics governing the behavior of individual cracks. The continuum models connect the evolution of elastic moduli with changes of crack density through a non-dimensional intensive damage variable characterizing material volumes large enough to allow smooth description of the distribution of internal flaws (micro-cracks in laboratory specimen).

Rabotnov (1988) related the damage variable to a reduction of the effective cross-section area that supports the load. Fiber-bundle models of damage (e.g., Newman and Phoenix, 2001) share that physical concept with cracks represented by torn fibers. Lyakhovsky and Myasnikov (1984, 1985), Lyakhovsky et al. (1997a, 1997b), Hamiel et al. (2004), and Lyakhovsky and Ben-Zion (2008) developed a thermodynamically-based non-linear continuum visco-elastic damage model for evolving elastic properties of rocks. Their model accounts for the following general aspects of brittle rock deformation: (1) non-linear elasticity that connects the effective elastic moduli to a damage variable and loading conditions. (2) Evolution of the damage state variable as a function of the ongoing deformation and gradual conversion of elastic strain to permanent inelastic deformation during material degradation. (3) Macroscopic brittle instability at a critical level of damage and related rapid conversion of elastic strain to permanent inelastic strain. This approach was adopted by Ben-Zion et al. (1999), Lyakhovsky (2001), Ben-Zion and Lyakhovsky (2002, 2006), and Lyakhovsky and Ben-Zion (2009) to study the evolution of geometrical and material properties of crustal fault zones, along with the evolution of various types of seismicity patterns.

The forgoing studies used quasi-static numerical simulations combined with selective analytical results. The obtained results were shown to be consistent overall with geological and seismological observations, as well as theoretical results associated with other frameworks (e.g., Ben-Zion, 2008). However, two simplifications in the previous formulation of the non-linear visco-elastic continuum damage rheology limit the model utility for studies of detailed irreversible deformation. These are (a) the *local* dependency of the energy function and related variables on damage, which leads for ranges of rheological parameters and boundary conditions to a singular localization (e.g., Lyakhovsky et al., 1997a; Lyakhovsky, 2001), and (b) the abrupt drop of the deviatoric stress during brittle failure, without any length or time scales, which renders the model inherently discrete in the sense of Rice (1993) and Ben-Zion and Rice (1995). The goal of the present paper is to provide a more detailed treatment of the energy function and reduction of the deviatoric stress during instabilities that will allow us to describe better the evolution and effects of rock damage in close spatio-temporal proximity to brittle failure events, along with aspects of wave propagation and dynamic rupture in damaged media.

Strong micro-crack interaction in a highly damaged area prior to total failure may be accounted for by adopting a non-local model, in which the constitutive law at a given position involves weighted averages of a state variable (or a thermodynamic force) over a certain neighborhood. Such a concept of non-local continuum was first introduced to model small-scale effects and heterogeneities in elastic solids (e.g., Eringen, 1966; Kroner, 1968; Bazant, 1991). Nonlocal theories, either of integral or gradient type (e.g., Bazant and Jirasek, 2002), are capable of reproducing size effects (e.g., Bazant, 2005). An integral-type nonlocal framework is a model in which the constitutive law at a point of a continuum involves weighted averages of a state variable (or the associated thermodynamic force) over a certain neighborhood of that point (e.g., Marotti de Sciarra, 2009). A gradient-type model takes non-locality into account by enriching the local constitutive relations with the first or higher gradients of some state variables or thermodynamic forces. Myasnikov et al. (1990) presented a formulation for energy and entropy balance equation for a gradient-type model. Adopting the gradient-type approach one should assume that the free energy of the damaged material is not only a function of the strain tensor and damage variable, but also of the strain rate tensor and gradient of damage variable. Modeling the dynamic evolution of strength near brittle instabilities of damaged solids can be done by recognizing that at some damage level materials become effectively granular, and that near brittle instability a damaged material may be viewed as consisting of a mixture of solid and granular phases.

The rest of the paper is organized as follows. In Section 2 we develop a generalized version of the non-linear visco-elastic continuum damage rheology with non-local dependency on damage and improved treatment of dynamic failure phenomena. In Section 3 we illustrate the results with several analytical solutions and numerical simulations. The results are summarized and discussed in Section 4. Details related to the thermodynamic formulation of the model and wave attenuation in the damage model are provides in two appendixes.

2. Theory

2.1. General thermodynamic formulation

To account for dynamic rupture process, we generalize the results of Lyakhovsky et al. (1997a) for damage evolution during irreversible brittle deformation. We follow the approach of irreversible thermodynamics (e.g., Onsager, 1931; Prigogine, 1955; Biot, 1955; Truesdell and Noll, 2004), which was successfully applied to kinetics of chemical reactions and phase transitions (e.g., Fitts, 1962; de Groot and Mazur, 1962) and served as a basis for variational methods of continuous media models (e.g., Sedov, 1968; Malvern, 1969; Berdichevsky, 2009).

The constitutive behavior of the material and flow rules controlling the kinetics of related irreversible processes is entirely defined by specification of two potentials. The first is the free energy, F, and the second is the dissipation function or local entropy production, Γ. The maximum entropy production principle dictates the flow rules for the kinetics of the irreversible processes. A visco-elastic damage model should account for local entropy production terms associated with different irreversible dissipative processes including heat transport, viscous stress relaxation and damage evolution (Appendix A). Assuming that these different physical processes are independent we maximize each term independently. Following Onsager (1931), who theoretically generalized the empirical laws of Fourier, Ohm, Fick, and Navier (see review by Martyushev and Seleznev, 2006), we represent the specific local entropy production as a product of thermodynamic fluxes and thermodynamic forces. For small deviations from equilibrium, the Onzager principle can be obtained from the maximum entropy production principle, the maximum dissipation rate of mechanical energy, or the von Mises principle (e.g., Ziegler, 1983; Martyushev and Seleznev, 2006). Below we first define the specific form of the energy function and then formulate the kinetic relations for damage evolution based on the Onsager principle.

The free energy of a solid in the local damage model of Lyakhovsky et al. (1997a) is assumed to be a function only of the local state variables, which are the temperature T, the elastic strain tensor $\varepsilon_{ij}=g_{ij}-g_{ij}^0$ (the difference between the total strain tensor g_{ij} and the irreversible strain tensor g_{ij}^0), and the damage variable α

$$F=F(T,\varepsilon_{ij},\alpha). \tag{1}$$

We extend the local constitutive relation (1) to a gradient-type non-local model by adding dependencies of F on the gradient of the damage state variable, $\nabla_i\alpha$, as well as on the strain rate tensor, $e_{ij}=dg_{ij}/dt$

$$F=F(T,\varepsilon_{ij},e_{ij},\alpha,\nabla_i\alpha). \tag{2}$$

The strain rate tensor as an additional thermodynamic state variable gives rise to the Jefferys model, which combines Maxwell and Kelvin–Voigt visco-elasticity (e.g., Rabotnov, 1988; Christensen, 2003). The spatial derivative of the damage state variable allows the formulation to account for strong interaction of internal flaws in a highly damaged region prior to total macroscopic failure.

The simplest extension of the previous local model discussed in Lyakhovsky et al. (1997a) to a gradient-type non-local isotropic model involves incorporating quadratic terms of the first-order time derivatives of strain and damage, along with the gradient of the damage state variable

$$F=\frac{1}{\rho}\left(\frac{\lambda}{2}I_1^2+\mu I_2-\gamma I_1\sqrt{I_2}+\eta\varepsilon_{ij}e_{ij}+\frac{\kappa}{2}\nabla_i\alpha\cdot\nabla_i\alpha\right), \tag{3}$$

where λ and μ are Lame constants, $I_1=\varepsilon_{ij}\delta_{ij}$ and $I_2=\varepsilon_{ij}\varepsilon_{ij}$ are the first and second invariants of the strain tensor ε_{ij}, γ is an additional modulus of a damaged solid, η is Kelvin–Voigt viscosity, and the additional dimensional coefficient κ characterizes the length scale of the non-local formulation.

The first two terms of (3) give the classical strain potential of linear elasticity (e.g., Malvern, 1969). The third term, which couples volumetric and shear strain, may be derived using the effective medium theory of Budiansky and O'Connell (1976) for non-interacting cracks that dilate and contract in response to tension and compression (Lyakhovsky et al., 1997b), or by expanding the strain energy potential as a general second-order function of I_1 and I_2 and eliminating terms that are either singular or not consistent with dilation during brittle deformation under shear loading (Ben-Zion and Lyakhovsky, 2006; Hamiel et al., in press). The non-analytic second order term with the modulus γ leads to non-linear elasticity for damaged material ($\alpha\neq0$, $\gamma\neq0$) even under infinitesimal strain. This term also produces gradual changes in the effective elastic moduli under non-proportional loading which become abrupt when the loading reverses from compression to tension. In addition to producing material dilation under shear loading, the damage model with energy function (3) can explain well various deformation, acoustic emission and wave propagation features observed in laboratory fracturing experiments with stiff rocks (e.g., Lyakhovsky et al., 1997b; Hamiel et al., 2005, 2009; Lyakhovsky and Ben-Zion, 2009; Lyakhovsky et al., 2009; Hamiel et al., in press).

The functional relation between the free energy (3) and the damage state variable is established by making the elastic moduli functions of α. With the current level of experimental constraints, some simple assumptions should be made. Agnon and Lyakhovsky (1995) assumed that the moduli μ and γ are linear functions of α and that λ is constant. Hamiel et al. (2004) reviewed this assumption and demonstrated that a power-law relation $\gamma(\alpha)$ improves the quality of fitting between laboratory measured stress–strain curves and model predictions. This power-law relation also leads to a transition between stable and unstable damage evolution in rocks (Hamiel et al., 2004). For mathematical simplicity we

adopt here the linear relations

$$\begin{aligned}&\lambda=\lambda_0,\\&\mu=\mu_0-\alpha\mu_r,\\&\gamma=\alpha\gamma_r,\end{aligned}\tag{4}$$

where λ_0, μ_0, and $\gamma=0$ are the elastic moduli of a damage-free material ($\alpha=0$), and $\lambda=\lambda_0$, $\mu=\mu_0-\mu_r$, and $\gamma=\gamma_r$ give the values of the moduli at maximum damage level ($\alpha=1$). During damage accumulation the modulus γ increases and the shear modulus μ decreases, corresponding to material evolution from linear elastic solid ($\alpha=0$) to strongly non-linear behavior and macroscopic brittle instability at some critical damage level (α_c). The conditions for the macroscopic instability will be discussed in the next section.

Taking the derivative of the energy form (3) with respect to the strain ((a14), Appendix A) leads to the following stress–strain relation:

$$\sigma_{ij}=(\lambda I_1-\gamma\sqrt{I_2})\delta_{ij}+\left(2\mu-\gamma\frac{I_1}{\sqrt{I_2}}\right)\varepsilon_{ij}+\eta e_{ij}-\kappa\nabla_i\alpha\cdot\nabla_j\alpha.\tag{5}$$

The obtained relation includes three different types of terms. The first two terms relate the stress to the elastic strain as in the local model. The third term is a usual extension of elasticity to Kelvin–Voigt visco-elasticity. This basic model is commonly used in seismology to describe observed attenuation or damping of seismic waves (e.g., Aki and Richards, 2002). The attenuation coefficient of propagating waves is proportional to the Kelvin–Voigt viscosity, or the seismic quality factor $Q=\rho v^2/\eta\omega$ with v and ω denoting elastic wave velocity and frequency. The physical mechanism of wave attenuation in damaged rocks, and general relation between crack density or damage variable and the attenuation coefficient, are discussed further in Appendix B. The last term in (5) defines the "structural stresses" associated with the heterogeneous damage distribution.

Using the energy Eq. (3), the specific local entropy production associated with the viscous deformation ((a10), Appendix A) has the form:

$$\Gamma_V=\frac{1}{T\rho}\left[\left(\lambda I_1-\gamma\sqrt{I_2}\right)\delta_{ij}+\left(2\mu-\gamma\frac{I_1}{\sqrt{I_2}}\right)\varepsilon_{ij}+\eta e_{ij}\right]\frac{dg_{ij}^{(0)}}{dt}-\frac{\eta}{T\rho}\varepsilon_{ij}\frac{de_{ij}}{dt}.\tag{6}$$

Relation (6) includes a Maxwell type shear heating term associated with gradual accumulation of irreversible deformation $g_{ij}^{(0)}$, and a Kelvin–Voigt type term describing entropy production proportional to the time-derivative of the strain rate tensor. The linear proportionality between the thermodynamic force ($dg_{ij}^{(0)}/dt$) and thermodynamic flux leads to a constant linear Newtonian viscosity. Following Maxwell visco-elastic rheology, the irreversible deformation may be represented as the sum of strain components associated with different deformation mechanisms. These may include dislocation creep, solid state diffusion, solution-diffusion-precipitation processes and other mechanisms (e.g., Kohlstedt et al., 1995; Regenauer-Lieb and Yuen, 2003). A power-law rheology is widely accepted for expressing the strain rate of dislocation flow (e.g., Weertman, 1978). A deformation mechanism associated with macroscopic material failure and transition to a granular flow will be discussed in Section 2.3.

Analysis of observed stress–strain curves and acoustic emission from laboratory experiments with granites and sandstones led Hamiel et al. (2004) to incorporate in the model a gradual damage-related Maxwell type inelastic deformation (creep) before the occurrence of macroscopic brittle failure. This inelastic strain $g_{ij}^{(0)}$ begins to accumulate with the onset of acoustic emission and the rate of its accumulation is assumed to be proportional to the rate of damage increase

$$\frac{dg_{ij}^{(0)}}{dt}=\begin{cases}C_V\frac{d\alpha}{dt}\sigma_{ij}^d & \frac{d\alpha}{dt}>0\\0 & \frac{d\alpha}{dt}\le 0\end{cases},\tag{7}$$

where C_v is a material constant and σ_{ij}^d is the deviatoric stress tensor. The effective compliance or inverse of viscosity ($C_v d\alpha/dt$) relates the deviatoric stress to the rate of irreversible strain accumulation. This model assumption implies that the total irreversible strain accumulated during loading should be proportional to the overall damage increase in the deforming rock sample.

Using the energy Eq. (3) combined with (4) into the local entropy production associated with the damage evolution term (a11) is

$$\Gamma_D=\frac{1}{T\rho}\left(\mu_r I_2+\gamma_r I_1\sqrt{I_2}-\frac{\partial\eta}{\partial\alpha}\varepsilon_{ij}e_{ij}+\kappa\nabla^2\alpha\right)\frac{d\alpha}{dt}.\tag{8}$$

Following Onzager (1931) principle, the linear relation between the thermodynamic force and flux leads to damage kinetics equation of the form:

$$\frac{d\alpha}{dt}=C\left(\mu_r I_2+\gamma_r I_1\sqrt{I_2}-\frac{\partial\eta}{\partial\alpha}\varepsilon_{ij}e_{ij}+\kappa\nabla^2\alpha\right),\tag{9}$$

where C is a positive constant or function of state variables. Eq. (9) is a second order parabolic (diffusion) equation with source terms. In the quasi-static case of gradual uniform damage evolution, associated with slowly changing elastic strains,

the second order spatial derivatives of the damage and the time derivative of the elastic strain may be neglected. With these simplifications, the equation for the kinetics of damage evolution is reduced to the equation derived by Lyakhovsky et al. (1997a) for the local damage rheology model:

$$\frac{d\alpha}{dt}=\begin{cases} C_d I_2(\xi-\xi_0), & \text{for} \quad \xi\geq\xi_0 \\ C_1\exp\left(\frac{\alpha}{C_2}\right)I_2(\xi-\xi_0), & \text{for} \quad \xi<\xi_0 \end{cases}, \tag{10}$$

where $\xi=I_1/\sqrt{I_2}$ is referred to as the strain invariants ratio. The parameter $\xi_0=-\mu_r/\gamma_r$ separates states of deformation involving material degradation and healing, associated with positive and negative evolution of damage, respectively. The parameter $C_d=C\gamma_r$ is a damage-rate constant for material degradation and it defines the timescale for the occurrence of macroscopic brittle failure following the onset of positive damage evolution at $\xi=\xi_0$. The rate of damage recovery for $\xi<\xi_0$ is assumed in (10) to depend exponentially on α. Lyakhovsky et al. (2005) showed that the local damage model reproduces the main phenomenological features of the rate- and state-dependent friction, and constrained the healing parameters C_1, C_2 by comparing the model calculations with empiric parameters of the frictional sliding (e.g., Dieterich, 1972, 1979; Marone, 1998).

2.2. Macroscopic failure

Two mathematically different conditions can be utilized for analyzing the macroscopic stability of solid under deformation. The first is convexity of the elastic strain energy, which is necessary for the existence of a unique solution of the static problem (e.g., Ekland and Temam, 1976). This criterion was adopted and expanded by Hill (1998), Truesdell and Noll (2004), and others in the framework of plasticity theory. The second is a change of the elasto-dynamic equation to ellipticity (e.g., Rudnicki and Rice, 1975). These two conditions are not always identical, especially for non-linear elasticity (e.g., Schreyer and Neilsen, 1996a, b). The first condition is a stronger one and convexity may be lost prior to the transition to ellipticity.

The condition of convexity of the elastic strain energy implies positivity of all the eigenvalues of the Hessian matrix ($\partial^2 U/\partial\varepsilon_{ij}\partial\varepsilon_{kl}$), providing a canonical base in the mathematical space of elastic deformations (ε_{11}, ε_{22}, ε_{33}, ε_{12}, ε_{13}, ε_{23}). The size of the Hessian matrix may be reduced to 3×3 components by rotating the coordinate system to the principal strain axes. In this case the matrix (Table 1) has three eigenvalues given in Lyakhovsky et al. (1997a). The conditions for the positivity of the eigenvalue are:

$$2\mu-\gamma\xi>0, \tag{11}$$

$$(2\mu-\gamma\xi)^2+(2\mu-\gamma\xi)(3\lambda-\gamma\xi)+(\lambda\gamma\xi-\gamma^2)(3-\xi^2)>0. \tag{12}$$

Condition (11) coincides with the condition for the positivity of the shear wave velocity, $V_s>0$, where $V_s^2=(\mu-\gamma\xi/2)/\rho$ (Hamiel et al., 2009). In this case, the convexity condition (11) coincides with the condition of the change of the elasto-dynamic equation to ellipticity (Fig. 1). This condition is dominant at relatively high positive values of ξ typical for tensile stresses. At lower ξ values, typical for fracturing under confining pressures, condition (12) becomes dominant and is stronger than the ellipticity condition. In addition to the limit associated with positivity of the shear wave velocity, $V_s=0$, Fig. 1 also shows a corresponding limit for positivity of a quasi-shear anisotropic wave, $V_{qs}=0$, which is the slowest wave for low ξ-values (Hamiel et al., 2009).

Macroscopic stability of a highly damaged solid with $\alpha=1$ can exist only if the strain invariants ratio is below its critical value, $\xi<\xi_0$ (Fig. 1). This stability condition formulated in terms of strain invariants is equivalent to the Schleicher yielding condition of the elasto-plastic model (Myasnikov and Oleinikov, 1991), which generalizes the von Mises yielding condition by making the critical stress value an arbitrary function of the mean stress (e.g., Hill, 1998). Extending such analyses, Lyakhovsky and Ben-Zion (2008) obtained a yielding condition for a damaged solid with $\alpha=\alpha_{cr}(\xi)$. These derivations provide connections between the stability condition (12) and internal friction at the critical state, $\alpha=\alpha_{cr}(\xi)$, and enable using the associated plasticity law of Drucker (1949) to solve quasi-static problems with the damage model. Fig. 1 (red line) shows that the lowest friction value ($\sim$0.25) is obtained for $\xi=\xi_0$ and $\alpha=1$. The friction at critical level of

Table 1
Hessian matrix ($\partial^2 U/\partial\varepsilon_{ij}\partial\varepsilon_{kl}$).

	ε_{11}	ε_{22}	ε_{33}	ε_{12}	ε_{13}	ε_{23}
ε_{11}	$\lambda+2\mu-\gamma\xi+\gamma\xi e_1^2-2\gamma e_1$	$\lambda-\gamma(e_1+e_2)+\gamma\xi e_1e_2$	$\lambda-\gamma(e_1+e_3)+\gamma\xi e_1e_3$	0	0	0
ε_{22}	$\lambda-\gamma(e_1+e_2)+\gamma\xi e_1e_2$	$\lambda+2\mu-\gamma\xi+\gamma\xi e_2^2-2\gamma e_2$	$\lambda-\gamma(e_2+e_3)+\gamma\xi e_2e_3$	0	0	0
ε_{33}	$\lambda-\gamma(e_1+e_3)+\gamma\xi e_1e_3$	$\lambda-\gamma(e_2+e_3)+\gamma\xi e_2e_3$	$\lambda+2\mu-\gamma\xi+\gamma\xi e_3^2-2\gamma e_3$	0	0	0
ε_{12}	0	0	0	$2\mu-\gamma\xi$	0	0
ε_{13}	0	0	0	0	$2\mu-\gamma\xi$	0
ε_{23}	0	0	0	0	0	$2\mu-\gamma\xi$

Here $e_i=\varepsilon_i/\sqrt{I_2}$ is a normalized value of the deformation along the principal axis "i".

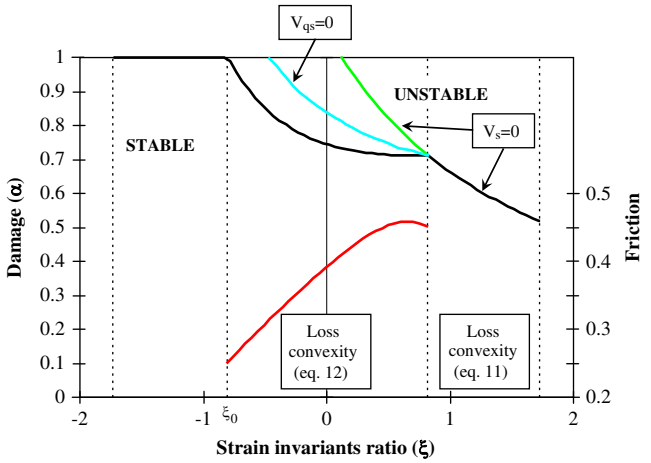

Fig. 1. Schematic diagram illustrating the critical level of damage versus the strain invariants ratio ($\xi = I_1/\sqrt{I_2}$) for $\lambda_0 = \mu_0$. The parameter ξ_0 prescribes the onset of damage accumulation. The material is stable for $\xi < \xi_0$. The black line corresponds to the condition of convexity loss, while colored lines represent the transition to ellipticity: green line for $V_s = 0$ and light blue line for $V_{qs} = 0$. The red line shows the effective coefficient of friction for $\alpha = \alpha_{crit}(\xi)$. (For interpretation of the references to color in this figure legend, the reader is referred to the web version of this article.)

damage, $\alpha = \alpha_{cr}(\xi)$, gradually increases with ξ under conditions where (12) is dominant. At higher ξ values at least one of the principal stress values becomes tensile; in this case the friction coefficient becomes irrelevant.

2.3. A transition to granular flow

In a simplified 1-D case, our model predicts that the effective elastic modulus for tension degrades significantly faster than the compressive one. At critical damage level the tensile modulus vanishes while the compressive modulus remains finite. This resembles the mechanical behavior of a cohesionless granular material where tensile stresses do not exist. Based on this analogy, Myasnikov and Oleinikov (1991) and Revugenko (2006) discussed a mathematical model of granular material as a limit case of media that react differently to tension and compression. Ben-Zion et al. (in press) proposed a mean field framework that can be used to study transitions between solid and granular states of material, and related different dynamic regimes, in terms of 3 tuning parameters: dynamic strength change during failure, the void fraction in granular materials and damaged solids, and the ratio of shear rate over healing rate. All these parameters are related directly or indirectly to cohesion. Following these ideas we suggest that the critical value of the damage state variable $\alpha_{cr}(\xi)$, corresponding to macroscopic brittle instability, is associated with a phase transition from a damaged solid to a granular material in the process zone around the generated macroscopic failure zone. In the vicinity of the critical state $\alpha = \alpha_{cr}(\xi)$, a mixture zone similar to a mushy region discussed in the context of the Stefan problem (e.g., Crank, 1987) is expected. Below we present a brief discussion of granular mechanics and suggest a simplified description for the transitional zone between solid and granular states.

Starting with pioneering works by von Mises and von Karman, several models involving yield conditions and flow rules have attempted to account for the observed solid- and fluid-like phenomenology of granular material (e.g., Jaeger et al., 1996; Liu and Nagel, 2001). Numerous models can reproduce basic features of quasi-static solid-like deformation in dense randomly packed granular media (e.g., Rao and Nott, 2008). The analysis of rapid granular flow (granular gas) with short duration interaction between particles is usually based on kinetic theory utilizing the Chapman–Enskog approach (e.g., Chapman and Cowling, 1964). A model that combines frictional and kinetic theories was proposed by Savage (1998). The model starts with a yield condition plus associated flow rule and accounts for fluctuations in the rate of the deformation tensor at any location about the mean value. The average stress tensor is determined by averaging over the entire range of deformation assuming that the strain rate fluctuations follow a Gaussian distribution. This assumption leads to Newtonian constitutive relations, with the bulk and shear viscosities related to a "granular temperature" which is a measure of the specific kinetic energy of the transitional velocity fluctuations (e.g., Savage, 1998). The transition to the solid-like phase in the dense regime where the granular material barely flows has been the subject of considerable research. Many recent studies suggested that "jamming transitions" may be used to classify behavior of a wide variety of physical systems, including critical slowdown in the granular flow dynamics before transition from fluid-like to solid-like behavior (e.g., Liu and Nagel, 1998; D'Anna and Gremaud, 2001; Trappe et al., 2001; Song et al., 2008; Chandelier and Dauchot, 2010).

Edwards and co-workers (Edwards and Oakeshott, 1989; Mehta and Edwards, 1989; Edwards, 1990, 2005; Makse et al., 2004) proposed a thermodynamic description of dense granular material consisting of a large number of dissipative particles that are massive enough so that their potential energy is orders of magnitude larger than their thermal energy. A central postulate of the Edwards theory is the existence of a new state variable called compactivity $\chi^{-1} = \partial S/\partial V$, instead of the temperature $T^{-1} = \partial S/\partial E$ in classical statistical mechanics (e.g., Landau and Lifshitz, 1980). The entropy is defined in

analogy to classical statistical mechanics as $S(V,N)=\lambda_E \ln(\Omega)$, where Ω is the number of mechanically stable configurations of N particles in a fixed volume V, and λ_E is the equivalent of the Bolzmann constant. Most formulas of the Edwards theory, including the Boltzmann distribution of the states of a system, are analogous to those of classical statistical mechanics, with some changes of variables. A number of recent theoretical and experimental studies provided evidence supporting the theory (e.g., Makse and Kurchan, 2002; Coniglio et al., 2004; Schroter et al., 2005; Metzger and Donahue, 2005; Briscoe et al., 2008; McNamura et al., 2009).

The Edwards theory, like classical statistical mechanics with the Boltzmann distribution of the states of a system, does not reproduce phase transitions which require more complex equation of state and another statistical distribution. For a system of identical particles, the average number of particles, n_i, in a state i, is given by the Fermi–Dirac distribution (e.g., Landau and Lifshitz, 1980)

$$n_i = \frac{1}{\exp(E_i - E_0/kT)+1}. \tag{13}$$

where k is the Boltzmann constant, T is the absolute temperature, E_i is the energy of state i, and E_0 is the energy at the critical state or chemical potential in a classical system. It is reasonable to assume that similar statistics may apply to granular material in the vicinity of the transition from a fluid-like to a solid-like state. Following ideas of the Edwards theory, the equivalent of the Bolzmann constant multiplied by the compactivity, $\chi\lambda_E$, should replace kT in (13), and an intrinsic state function should replace the energy. We therefore assume that the probability P that a material element (particle) of the mixture zone (mushy region) in the vicinity of the critical state, $\alpha=\alpha_{cr}(\xi)$, is in a solid state has a functional form similar to (13)

$$P(\alpha) = \frac{1}{\exp(\alpha - \alpha_{cr}(\xi)/\beta)+1}. \tag{14}$$

The probability of being in a granular state is given by $(1-P)$ and the β-value defines the width of the transitional region. For $\beta\to 0$, $P(\alpha)$ approaches the Heaviside (step) function that abruptly changes its value from zero to one. In this case the transition from the solid to granular state is abrupt without any mushy region. While these results should be followed by more detailed analyses, they provide general guidelines for describing the deformation processes near the unstable regime $\alpha\to\alpha_{cr}(\xi)$.

3. Analytical and numerical results

We now present four different model solutions demonstrating the main features of the formulated model. We start with quasi-static damage evolution under constant stress, which is the simplest model demonstrating the Kelvin–Voigt damage-dependent retardation of instability. The second solution emphasizes the non-local features of the model by analyzing damage localization under constant shear strain. Next, we address damage diffusion and simulate size effect in mode-I crack driven by remote tension. These solutions are obtained for the "elastic" damage model that ignores gradual accumulation of the irreversible strain (Maxwell terms). In this case the strain rate tensor is equal to the time derivative of the elastic strain tensor ($e_{ij}=d\varepsilon_{ij}/dt$). The complete model formulation is applied in the last case dealing with deformation and damage evolution of the material in a narrow zone subjected to constant compacting strain and increasing shear strain due to motion of outer elastic blocks.

3.1. Damage evolution in a uniform block under constant loading

In a 1-D case the effective elastic modulus G degrades proportionally to the damage increase, $G(\alpha)=G_0(1-\alpha)$, and the stress–strain constitutive relation is

$$\sigma = G_0(1-\alpha)\varepsilon + \eta(\alpha)\frac{d\varepsilon}{dt}. \tag{15}$$

Neglecting the gradient damage terms for a homogeneous damage evolution, the equation for the damage evolution reduces to

$$\frac{d\alpha}{dt} = C_d\varepsilon^2 - \frac{C_d}{G_0}\frac{\partial\eta}{\partial\alpha}\varepsilon\frac{d\varepsilon}{dt}. \tag{16}$$

Assuming constant stress σ and neglecting the Kelvin–Voigt viscosity terms, $\eta(\alpha)=0$, leads to a power law damage accumulation previously discussed by Ben-Zion and Lyakhovsky (2002) and Turcotte et al. (2003)

$$\alpha(t) = 1 - \left(1 - 3\frac{C_d\sigma^2}{G_0^2}t\right)^{1/3}. \tag{17}$$

This solution predicts acceleration of seismic energy release prior to the occurrence of strong brittle events, with time-to-failure, t_f, given by

$$t_f = \frac{G_0^2}{3C_d\sigma^2}. \tag{18}$$

The rate of damage growth increases monotonically and goes to infinity toward the macroscopic failure, $d\alpha/dt \to \infty$ for $t \to t_f$ and $\alpha \to 1$.

Following relation (B2) between the attenuation coefficient and the observed damage in rock samples, and recalling the proportionality between attenuation of waves and Kelvin–Voigt viscosity, we prescribe $\eta(\alpha)$ as

$$\eta(\alpha) = \eta_1 + \frac{\eta_2}{\alpha_{cr}-\alpha}, \tag{19}$$

where the critical level of damage in the 1-D case is $\alpha_{cr}=1$. Substituting (19) into (15) and (16), leads to the following system of two coupled first order differential equations for strain and damage evolution:

$$\frac{d\varepsilon}{dt} = (1-\alpha)\frac{\sigma - G_0(1-\alpha)\varepsilon}{\eta_1(1-\alpha)+\eta_2}, \tag{20}$$

and

$$\frac{d(1-\alpha)^2}{dt} = -2C_d\varepsilon^2(1-\alpha) + 2\frac{C_d}{E_0}\eta_2\varepsilon\frac{\sigma - G_0(1-\alpha)\varepsilon}{\eta_1(1-\alpha)+\eta_2}. \tag{21}$$

In contrast to (17), the solution of Eqs. (21) and (22) predicts that the strain rate and the rate of damage accumulation go to zero ($d\varepsilon/dt \to 0$, $d\alpha/dt \to 0$) toward the macroscopic failure ($\alpha \to 1$). The analytical asymptotic solution for infinite time ($t \to \infty$) has the following form:

$$\begin{aligned} \varepsilon(t) &= a\sqrt{t} \\ \alpha(t) &= 1 - \frac{b}{\sqrt{t}}, \end{aligned} \tag{22}$$

with coefficients a and b given by

$$\begin{aligned} a &= \frac{2\sigma b}{\eta_2 + 2G_0 b^2}, \\ b &= \sqrt{\frac{1}{2}\frac{\eta_2}{G_0}}. \end{aligned} \tag{23}$$

This solution is obtained by neglecting higher order terms of time ($1/\sqrt{t}$, $1/t$, etc.) in the asymptotic expansion for $t \to \infty$. The asymptotic solution (22) for the damage and strain evolution means that it takes an infinite time to achieve a static macroscopic failure condition ($\alpha = 1$). Only in the case of $\eta = const.$, the rate of damage accumulation gradually increases, leading to macroscopic failure with a finite time-to-failure. In the more realistic case accounting for the damage-related increase of the Kelvin–Voigt viscosity parameter, the rate of damage accumulation increases up to some maximum value and then decreases.

Fig. 2 shows the damage evolution obtained by numerical solutions of (20, 21) together with the analytical solution (17) for $\eta = 0$ (red line). Time in the figure is normalized to the time to failure t_f (18). The simulation starts with a damage free material ($\alpha = 0$). The constant stress condition corresponds to initial strain of $\varepsilon(0) = \sigma/G_0 = 10^{-2}$; the value of η_1 in (19) is equal $10^{-2}G_o$ corresponding to a quality factor $Q = 10^2$ for intact rock and 1 Hz frequency. The blue, green, and purple lines correspond to $\eta_2 = 10\eta_1$, $30\eta_1$, and $50\eta_1$, respectively. The numerical solutions follow the analytical curve until the vicinity of the failure at time $t = t_f$. The differences between the analytical solution without damping and numerical solutions with damping terms are clearly seen in the inset figure. Instead of reaching the critical value of damage ($\alpha = 1$), as the analytical (red) line does, the solutions with damping become strongly bent and the damage remains below one for infinite time. This behavior is predicted by the asymptotic analytical solution (22) and shown in Fig. 3 (dashed line) together with the numerical solution. The numerical solution approaches the asymptotic value very fast and the solutions become almost identical to (22) already at time $t \sim 2\ t_f$ for relatively high η_2 value, and even faster for lower values (not shown here). The analytical solution can be used to define a scaling value $\Delta\alpha$

$$\Delta\alpha = \left(C_d\varepsilon^2\frac{\eta_2}{G_0}\right)^{1/3}, \tag{24}$$

that characterizes the expected distance from the critical damage value for times of the order of the time-to-failure t_f of (18).

Fig. 4 shows the rate of damage growth versus damage for different values of damping. At relatively low values of damage below ~ 0.7, all solutions (with or without damping) are almost identical. At higher values, the solutions for damped systems achieve maximum rate of damage growth close to the time-to-failure, t_f; and then strongly decreases toward zero. Fig. 5 shows the system behavior under different levels of loading. The parameters of the model with low stress are the same as for the solutions shown in Figs. 2 and 4 ($\eta_2 = 10\eta_1$). The curves with higher loading level correspond to stress values that are increased by factor two and three.

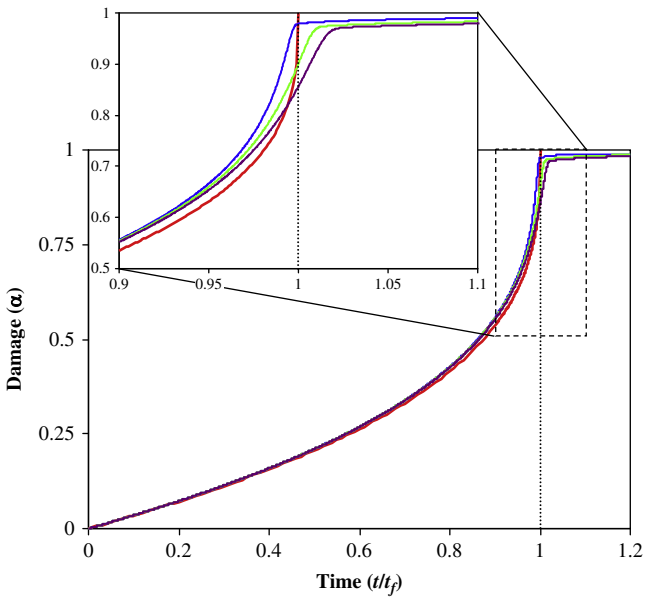

Fig. 2. Damage growth under constant load. The red line describes the analytical solution for $\eta=0$. The blue, green and violet lines correspond to $\eta_2=10\eta_1$, $30\eta_1$ and $50\eta_1$, respectively. (For interpretation of the references to color in this figure legend, the reader is referred to the web version of this article.)

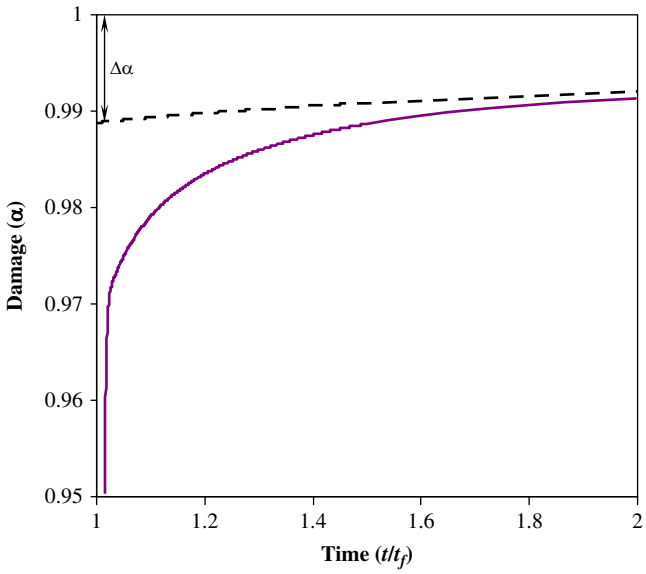

Fig. 3. Damage growth under constant load. The violet line is the same as in Figure 2 ($\eta 2=50\eta 1$) and the dashed line shows the asymptotic analytical solution. (For interpretation of the references to color in this figure legend, the reader is referred to the web version of this article.)

The asymptotic analytical solution (22) as well as the various numerical solutions discussed above demonstrate that the static failure condition ($\alpha=1$ in the 1-D case) corresponding to the loss of convexity is unreachable. We suggest that at some rate of damage increase (schematically shown by the dashed line in Fig. 5) the quasi-static solution is no longer valid and inertial terms should be incorporated to describe the dynamics of the system. However, before we discuss the transition to dynamic failure, we present additional quasi-static solution demonstrating the spatial distribution of damage and its localization under shear loading.

3.2. *Damage evolution in a non-uniform block under constant shear strain*

Basic aspects of the model behavior can be illustrated by examining the damage evolution in a long strip subjected to constant shear strain. We consider a strip with width L of 2 units, extending along the x-axis from -1 to 1 (Fig. 6). Fixed

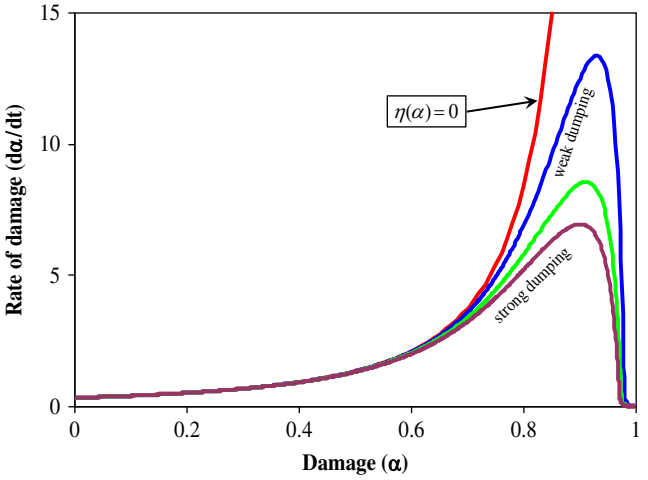

Fig. 4. The rate of damage growth versus damage in simulations with constant loading and different dumping factors. The model parameters are the same as for the violet line in Fig. 2. (For interpretation of the references to color in this figure legend, the reader is referred to the web version of this article.)

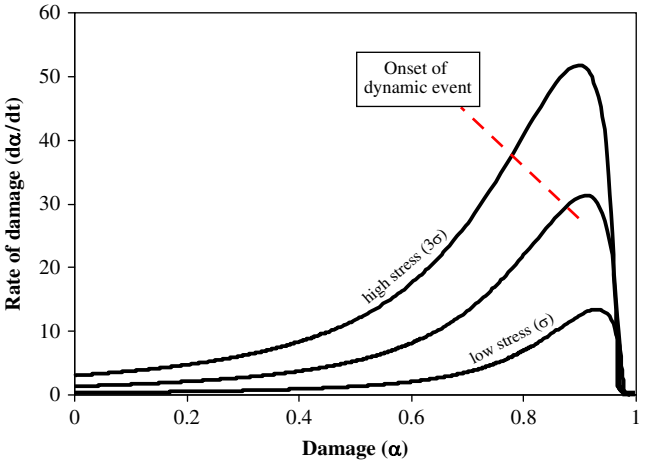

Fig. 5. The rate of damage growth versus damage in simulations under constant loadings with different stress levels and $\eta_2=10\eta_1$. The red dashed line represents the dynamic failure condition. (For interpretation of the references to color in this figure legend, the reader is referred to the web version of this article.)

displacements at the edges, $u|_{x=\pm 1}=\pm u_0$, in the direction of the strip, enforce constant total shear strain. We assume that all functions describing material properties, damage and displacement depend only on the *x*-coordinate. This formulation is similar to the 1-D case discussed in Section 3.1 with the same stress–strain relation (15). Since the damage is function of time and x-coordinate, the structural stresses ($\nabla_i\alpha\cdot\nabla_j\alpha$) contribute only to the *xx*-component of the stress tensor. A quasi-static solution for the equation of motion, without body forces and neglecting the inertial terms, involves shear stress that is homogeneous in space and depends only on time. The integral of the strain $\int_{-1}^{1}\varepsilon dx=2u_0=const.$ represents the total shear strain of the zone which remains constant. Hence, its time derivative is zero and the shear stress may be expressed as

$$\tau=2G_0\frac{\int_{-1}^{+1}((1-\alpha)\varepsilon/\eta(\alpha))dx}{\int_{-1}^{+1}(dx/\eta(\alpha))}. \tag{25}$$

Substituting (25) into (15) eliminates the stress from the equations and leaves only two unknowns, strain and damage.

Eq. (9) for the damage evolution of the non-local model includes a Laplacian term. In the 1-D case of a heterogeneous system, the second spatial derivative of the damage should be added to Eq. (16) for damage evolution

$$\frac{\partial\alpha}{\partial t}=C_d\varepsilon^2-\frac{C_d}{G_0}\frac{\partial\eta}{\partial\alpha}\varepsilon\frac{d\varepsilon}{dt}+D\frac{\partial^2\alpha}{\partial x^2}, \tag{26}$$

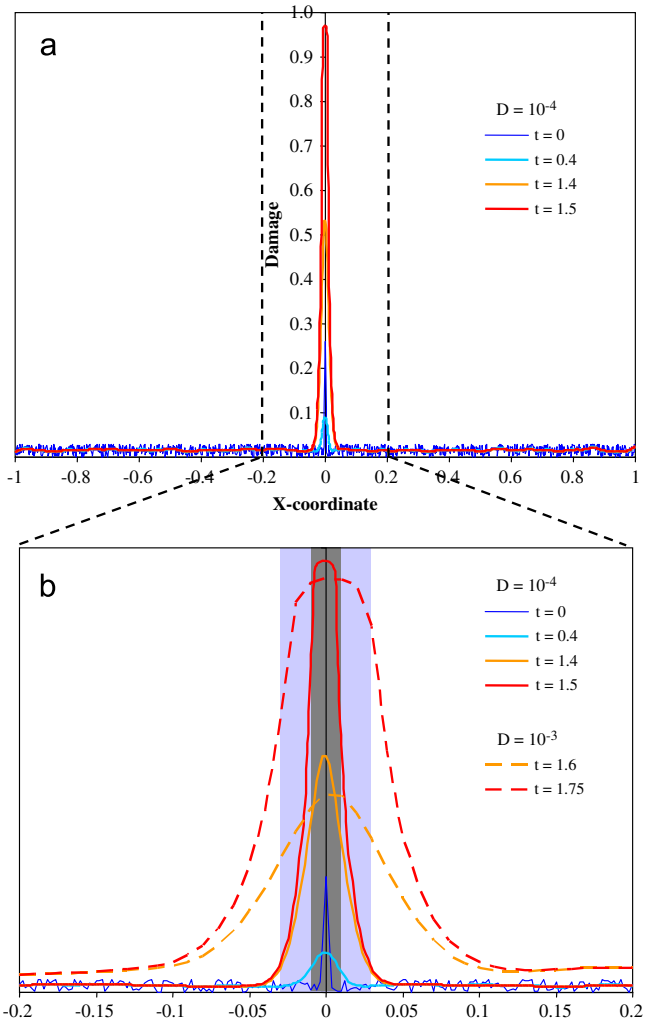

Fig. 6. (a) Width of a newly created damage zone under fixed displacement at the block boundaries. (b) Snapshots of simulated damage profiles around the localization zone for two different values of the damage diffusion coefficient. The size of the shaded areas corresponds to the analytically predicted width of the damage zone. (For interpretation of the references to color in this figure, the reader is referred to the web version of this article.)

where $D=\kappa C_d/G_0$ is the coefficient of damage diffusion. The "diffusion" term describes damage de-localization and it leads to a finite nonzero width of the newly created damage zone. Even if the initial damage is localized to a point, the final width of the damage zone, w, scales with the square root of time

$$w=\sqrt{Dt_f}. \tag{27}$$

The time-to-failure, t_f (18), is calculated in this case according to the applied stress at $t=0$.

The first order differential Eq. (15) for the strain evolution (using 25), combined with the second order parabolic Eq. (26) for the damage evolution, is solved numerically using explicit-in-time finite difference scheme for a given initial distribution of the damage $\alpha(x,0)$. Fig. 6 demonstrates the damage distribution at different evolutionary stages. The time is scaled to the time-to-failure, t_f. The initial damage (dark blue line in Fig. 6a) is randomly distributed between zero and 3×10^{-2}, except in a narrow "notch" around the point $x=0$ with maximum value of damage $\alpha(0,0)=0.25$. In the local damage models, without the spatial derivative term in the kinetic Eq. (26), this notch grows and produces strong strain and damage localization (e.g., Lyakhovsky et al., 1997a). In the non-local model, damage diffusion leads to significant widening of the notch that lasts about $t/t_f\sim0.4$ for $D=10^{-4}$ (D is scaled to half width of the zone and t_f). During this initial stage the level of damage in the center of the notch, $\alpha(0,t)$, decreases. This is shown in Fig. 7 by black, blue and red lines that can hardly be distinguished at this stage. When the spatial damage distribution is smoothed enough, the diffusion is less efficient and the positive source term associated with applied deformation overcomes the diffusion.

The rate and overall damage decrease during the initial stage are controlled by the diffusion coefficient (green line in Fig. 7a for $D=10^{-3}$). The rate of damage increase during later stages is affected by the damage-dependent Kelvin–Voigt

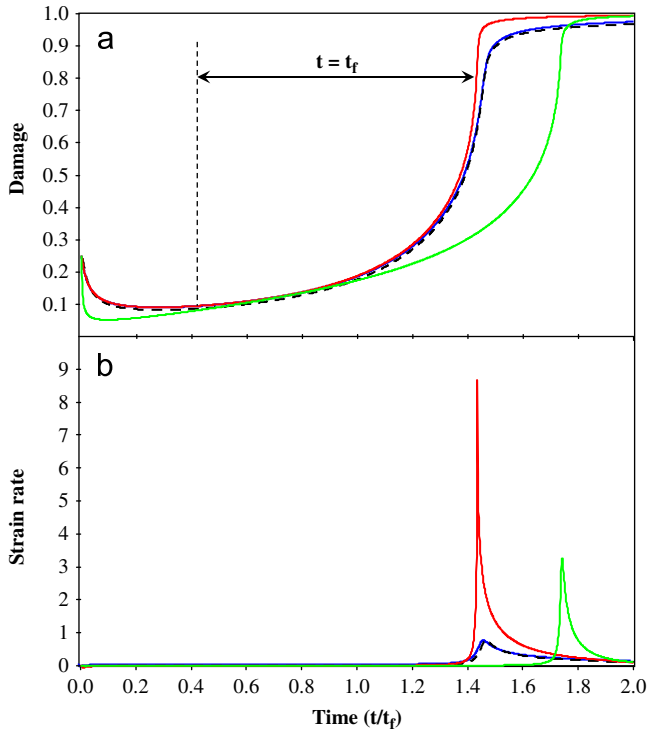

Fig. 7. Simulated damage (a) and strain rate (b) versus time in the center of a newly created damage zone ($x=0$). The curves are plotted for several values of D normalized to unit length and t_f; η_1 η_2 normalized to G_0 and t_f. The employed parameters are: red line—$D=10^{-4}$, $\eta_1=\eta_2=10^{-3}$; green line—$D=10^{-3}$, $\eta_1=\eta_2=10^{-3}$; blue line—$D=10^{-4}$, $\eta_1=\eta_2=10^{-2}$; dashed black line—$D=10^{-4}$, $\eta_1=10^{-3}$ $\eta_2=10^{-2}$. (For interpretation of the references to color in this figure legend, the reader is referred to the web version of this article.)

viscosity term in the stress–strain relation. However, variations in η_1 and η_2 values in (19) have minor effects on the evolving spatial damage distribution. The width of the damage zone remains about constant during the subsequent damage evolution (see red and orange lines for $t/t_f=1.4$ and 1.5 in Fig. 6a). The expanded gray region in Fig. 6b marks the width of the damage zone calculated using the scaling relation (27). The dashed lines in Fig. 6b show the damage distribution simulated with $D=10^{-3}$. The light blue region corresponds to a wider zone predicted by the scaling relation (27) for higher diffusion. This comparison shows that the damage mostly grows in a zone with width controlled by the damage diffusion coefficient and that relation (27) may be used for estimating the diffusion coefficient from laboratory experiments and field observations.

Damage increase toward macroscopic failure leads to an increase in the Kelvin–Voigt viscosity (19), which acts to stabilize the system. Similar to the model solution discussed in the previous section, viscosity increase leads to decrease in the rate of damage accumulation and prevents achieving the static failure condition ($\alpha=\alpha_c$). After a period of fast damage growth in the center of the notch ($x=0$), the process decelerates and the damage asymptotically approaches its critical value ($\alpha\to\alpha_c$). The duration of the period of the damage accumulation with slow diffusion ($D=10^{-4}$) and low damping ($\eta_1=\eta_2=10^{-3}$ $G_o t_f$) is very close to $t=t_f$ (red line in Fig. 7a), and is slightly longer ($t\sim 1.5t_f$) for the same damping but faster diffusion (green line in Fig. 7a for $D=10^{-3}$). At the final stage of evolution the rate of damage growth is significantly affected by the value of η_2 (blue and red lines in Fig. 7). In contrast, the rate of damage growth is hardly affected by the value of η_1 (black dashed and blue lines in Fig. 7).

The damage growth in a narrow zone leads to strain localization in a strip with width of about w (27). Even with complete stress drop, the final strain, ε_f, accumulated in the damage zone is proportional to the initial strain ε_0 of the zone multiplied by the ratio between model size and damage zone width

$$\varepsilon_f=\varepsilon_0\frac{L}{w}=\frac{u_0}{w}. \tag{28}$$

Relations (27) and (28) demonstrate that the width of the damage zone remains finite and the strain distribution is regular over the entire domain. These results differ from those obtained from the local damage rheology predicting $w\to 0$ and $\varepsilon_f\to\infty$ (e.g., Lyakhovsky et al., 1997a). The rate of strain accumulation in the damage zone significantly changes with the damage evolution. During most of the duration of damage growth the strain rate remains very low (Fig. 7b). It rapidly accelerates at the stage corresponding to fast damage accumulation and gradually decreases during damage deceleration. Fig. 7b (red line) shows that the largest strain rate is obtained for the low diffusion and low damping. An order of magnitude increase in the η_2 value (blue and dashed black lines) leads to about an order of magnitude reduction in the

strain rate. Intermediate strain rate reduction (green line) is obtained for low damping and high damage diffusion. The discussed quasi-static model solution becomes invalid when the strain-rate values are sufficiently high to produce elastic waves that propagate away from the newly created damage zone. This feature is addressed in the next section.

3.3. Size effect and quasi-static mode-I crack growth

Lyakhovsky (2001) addressed size-effect in mode-I crack driven by remote tension and internal pressure using local damage model (no damage diffusion). For a given ratio between internal pressure and remote tension, the simulated rate of crack propagation follows the empirical power law equation $dL/dt \propto L^n$ of Charles (1958) or the Paris and Erdogan (1963) law with power index $n \geq 1$. At small values of the internal pressure, the self-similarity becomes complete in terms of Barenblatt (1996) with the power index $n=1$. In this section we compare previous results with local damage model (Lyakhovsky, 2001) to the non-local formulation that includes damage diffusion.

The local damage rheology model provides a time scale for failure, t_f of Eq. (18), associated with the rate of damage accumulation. The non-local model includes a diffusive term in the damage evolution (9) that gives rise to additional characteristic time. The damage diffusive time scale, associated with the structural length scale or initial crack size L, is

$$t_D = \frac{L^2}{D}. \tag{29}$$

Therefore, the non-local model accounts for a competition between delocalization due to damage diffusion and localization due to loading. Using the expression for damage diffusion, $D = \kappa C_d/G_0$, the ratio between the time-to-failure, t_f (18), and damage diffusive time scale, t_D (29), is

$$D_D = \frac{t_f}{t_D} = \frac{\kappa G_0}{3\sigma^2 L^2}. \tag{30}$$

The damage diffusivity ratio, D_D, may be viewed as a measure for the material non-locality reflecting the role of the diffusion-controlled delocalization.

Fig. 8 shows numerical results of quasi-static growth of mode-I crack driven by remote tension (zero internal pressure) under conditions corresponding to two order of magnitude difference in the D_D value, between 10^{-2} and 10^{-4}, as well as local model, $D_D=0$. The simulations employ the numerical algorithm of Lyakhovsky (2001), modified for damage diffusion. Each simulation starts with a pre-existing unit notch placed in the damage-free material and ends when the crack approximately doubles its size. The non-dimensional crack velocity $(t_f/L_0)(dL/dt)$ increases with the crack length (Fig. 8). In the local model ($D_D=0$), after initial adjustment ($L/L_0 \sim 1.2$) the shape of the damage zone becomes self-similar (see Fig. 5 from Lyakhovsky, 2001) and the rate of the crack growth is proportional to its length ($dL/dt \propto L$). Certain rate-length scaling is also obtained with the non-local model. For $D_D=10^{-4}$ the slope of the rate-length curve is below the predictions of the local model and remains about constant for length values between 1.2 and 1.6. With increase of the crack length, the damage diffusivity ratio (30) decreases, diminishing the role of the non-locality and leading to an increase of the slope of the rate-length curve. For larger cracks ($L/L_0 > 2$, $D_D < 0.25 \times 10^{-4}$) the slopes of the local and non-local model curves are almost identical. Similar tendency is obtained for $D_D=3 \times 10^{-3}$ and $D_D=10^{-3}$, but the range of the lengths corresponding to linear scaling significantly extends. For $D_D=10^{-2}$ (not shown), the damage diffusion is very efficient, leading to fast blunting of the crack tip, which eliminates the stress concentration around the crack tip and prevents the crack growth.

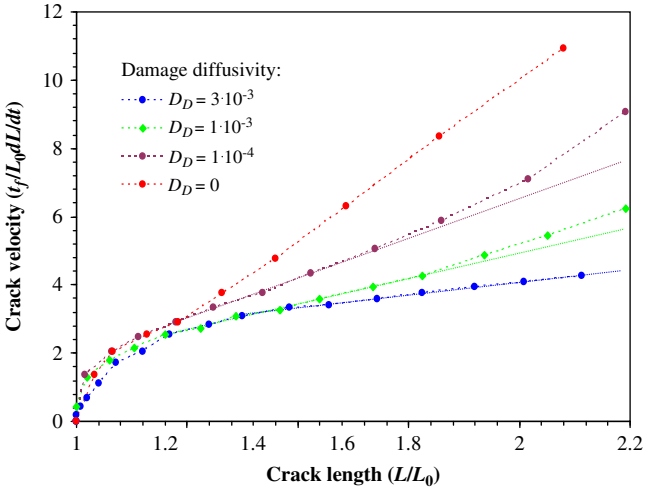

Fig. 8. Rate of quasi-static mode-I crack growth versus its length for different damage diffusivity ratios and local damage rheology model formulation. See text for additional explanations.

For mode-I crack growth driven by remote tension, the modeling results (Fig. 8) predict two end-member damage diffusivity values controlling the style of the crack behavior

(i) For small D_D values ($D_D < 0.25 \times 10^{-4}$) damage diffusivity is negligibly small and crack growth is described by the local damage model (Lyakhovsky, 2001) with linear scaling between the crack growth rate and its length ($dL/dt \propto L$). This scaling is compatible with the classical power law scaling between stress and crack length ($\sigma \propto L^{-1/2}$) of the linear elastic fracture mechanics.
(ii) For large D_D values ($D_D > 10^{-2}$) damage diffusivity is very efficient and prevents crack growth. Thus, a threshold D_D value can be defined for the onset of crack growth. Using this threshold value together with Eq. (30) yields a reciprocal relation between stress and crack length, $\sigma \propto L^{-1}$, consistent with a size effect for failures at crack initiation (e.g., Bazant, 2005).

3.4. Damage evolution in a long narrow zone under constant remote shear velocity

In this section we discuss a simplified model describing the transition from quasi-static evolution to dynamic slip event. Slip during earthquakes occurs primarily within relatively long and thin damage zone with width of 10^{-3}–10^{-5} m (e.g., Chester et al., 1993; Heermance et al., 2003; Rockwell and Ben-Zion, 2007). Therefore, we consider the deformation process associated with a uniform narrow damage zone between two moving elastic blocks (see Fig. 9 for notation). The material in the damage zone is subjected to constant compaction, ε_c, and increasing shear strain due to motion of the outer elastic blocks. The total shear strain, ε_t, of the damage zone is the sum of reversible elastic component, ε, and irreversible (viscous) component ε_v. The total shear strain is equal to the displacement at the edge of the damage zone divided by its width

$$\varepsilon_t = \varepsilon + \varepsilon_v = \frac{u(t)}{w}. \tag{31}$$

We define an irreversible (viscous) displacement component, $u_v = \varepsilon_v w$, and related irreversible strain rate $e = d\varepsilon_t/dt = (1/w)(du(t)/dt)$. With this notation, the elastic strain, its invariants and ratio of the strain invariants are

$$\begin{aligned} &\varepsilon = \frac{u(t) - u_v(t)}{w} \\ &I_1 = 3\varepsilon_c \\ &I_2 = 3\varepsilon_c^2 + 2\varepsilon^2 \\ &\xi = \frac{I_1}{\sqrt{I_2}} = \frac{3\varepsilon_c}{\sqrt{3\varepsilon_c^2 + 2\varepsilon^2}}. \end{aligned} \tag{32}$$

For a uniform time-dependent damage, $\alpha(t)$, the structural stresses ($\nabla_i\alpha \cdot \nabla_j\alpha$) are zero and the stress–strain relation for the shear stress component, τ, in the damage zone is

$$\tau = (2\mu(\alpha) - \gamma(\alpha)\xi)\varepsilon + \eta(\alpha)e. \tag{33}$$

In a 1-D case with $\varepsilon_c = const.$ the conditions of convexity of the elastic strain energy (11) and (12) are reduced to

$$\frac{\partial \tau}{\partial \varepsilon} = 2\mu(\alpha) - \gamma(\alpha)\xi - \gamma(\alpha)\frac{\partial \xi}{\partial \varepsilon} = 0. \tag{34}$$

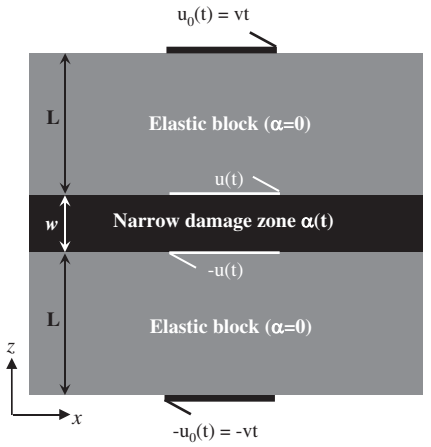

Fig. 9. Geometry and notations of a model setup for uniform narrow damage zone between two purely elastic blocks moving with constant velocity.

The condition of convexity (34) together with the linear connections between the elastic moduli and damage (4) lead to explicit relation for the γ_r value and critical damage $\alpha_{cr}(\xi)$

$$\gamma_r = \frac{6\mu_0}{\xi_0^3 - 6\xi_0}$$
$$\alpha_{cr}(\xi) = \frac{\xi_0^3 - 6\xi_0}{\xi^3 - 6\xi_0}. \tag{35}$$

The rate of damage accumulation (9) for the case of uniform damage distribution ($\nabla\alpha = 0$) combined with relations (10) and (19) yields

$$\frac{d\alpha}{dt} = \begin{cases} C_d I_2(\xi - \xi_0) - \frac{C_d}{\mu_0}\frac{\eta_2}{(\alpha_{cr}-\alpha)^2}\varepsilon e, & \text{for} \quad \xi \geq \xi_0 \\ C_1 \exp\left(\frac{\alpha}{C_2}\right) I_2(\xi - \xi_0), & \text{for} \quad \xi < \xi_0. \end{cases} \tag{36}$$

Two different mechanisms of irreversible strain accumulation are considered here. One is gradual accumulation of damage-related irreversible strain with rate proportional to the rate of damage accumulation (7). The other is associated with the transition from the damaged solid phase to the granular phase, and formation of a "mushy region" in the vicinity of the critical level of damage, $\alpha = \alpha_{cr}(\xi)$. The effective compliance or inverse of material viscosity of the mushy region is equal to zero for the solid state and gradually increases with $(1-P)$, the probability of being in a granular state (14)

$$\frac{d\varepsilon_v}{dt} \equiv \frac{1}{w}\frac{du_v}{dt} = C_v \tau \frac{d\alpha}{dt} + C_g \tau (1 - P(\alpha)), \tag{37}$$

where C_g is the compliance of a granular material ($\alpha = \alpha_{cr}$ and $P = 0$). The viscosity of the granular material is not necessarily constant, but is rather related to the "granular temperature" and the structure of the granular material (e.g., Savage, 1998). However, as a first approximation we assume a constant C_g. Since we discuss a low-temperature brittle behavior, we ignore temperature-activated ductile flow mechanism.

Eqs. (33), (36), and (37) define the evolution of the damage zone for prescribed loading at its edges. This loading is calculated using the stress distribution in the outer purely-elastic blocks. The displacements inside the blocks, $u_b(z,t)$, may be represented as a sum of two different components:

$$u_b(z,t) = \left[u_0(t)\frac{z - w/2}{L} - u(t)\frac{z - (L + w/2)}{L}\right] + u_S(z - V_S t). \tag{38}$$

The term enclosed in the square brackets stands for linear interpolation between displacements at the edges, $u(t)$ and $u_0(t)$, which is the static solution of linear elasticity. During the periods of fast damage accumulation and high strain rates in the damage zone, shear waves may be generated and propagate away from the damage zone. The term $u_S(z - V_s t)$ represents a planar shear wave traveling with velocity V_s. The employed signs hold for the upper block, and opposite signs should be applied for the lower block. Taking the spatial derivative of the displacement (38) and using $\partial u_S/\partial z = -(1/V_s)(\partial u_S/\partial t)$, the shear stress at the interface between the block and the damage zone, τ_b, is

$$\tau_b = \mu_0\left(\frac{u_0(t) - u(t)}{L} - \frac{1}{V_S}\frac{\partial u(t)}{\partial t}\right); \tag{39}$$

The first term stands for static elasticity and the second is usually referred to as radiation damping (e.g., Rice and Ben-Zion, 1996). Balancing the stresses at the interface between the elastic block (39) and the damage zone (33) leads to a final equation describing evolution of the entire system

$$\mu_0\left(\frac{u_0 - u}{L} - \frac{1}{V_S}\frac{du}{dt}\right) = (2\mu(\alpha) - \gamma(\alpha)\xi)\frac{u - u_v}{w} + \eta(\alpha)\frac{d}{dt}\left(\frac{u}{w}\right). \tag{40}$$

The obtained set of Eqs. (33), (36), (37), (40) fully defines the evolution of the system for given initial conditions and block velocity. These equations are solved numerically for different evolutionary scenarios discussed below.

The numerical simulations are done for a model size of $L = 10^4$ m which is several orders of magnitude larger than the width of the damage zone (10^{-3}–10^{-5} m) discussed above. To make the simulations more stable and efficient, we use $w = 10^{-3}$ m. Typical values for the elastic moduli of intact crystalline rocks are $\lambda_0 \sim \mu_0 \sim 10^{10}$ Pa. Characteristic values of the parameters controlling the onset of damage and its kinetics, constrained from previous laboratory studies (e.g., Hamiel et al., 2004; Lyakhovsky et al., 2005), are $\xi_0 = -0.8$, $C_d = 10$/s, $C_1 = 10^{-14}$/s, and $C_2 = 0.02$. The parameters C_1, C_2 are not well resolved, but their precise values play a minor role here since the details of the healing process affect primarily studies with multiple failure cycles. The expected slip velocity during seismic events is of the order of meter per second and the estimated shear stress in the seismogenic zone is of the order of 10–100 MPa (e.g., Ben-Zion, 2001). These values can be used to estimate the lower limit of the viscosity of the granular material in the damage zone, which can be as low as 10^2 Pa s and correspond to $C_g = 10^{-2}$/Pa s. The values of the viscosity coefficient η_2 (19) and parameter β (14) controlling the transition between solid and granular states are not well constrained. Therefore, we analyze the role of these parameters by varying their values in the range: $\eta_2 = 10^2$–10^4 Pa s and $\beta = 10^{-2} - 10^{-3}$.

The initial conditions of the numerical simulations correspond to zero damage and shear stress. A long-term quasi-static stress accumulation starts with the onset of the block motion. For typical tectonic velocities associated with plate motion (millimeters to centimeters per year), it takes years to accumulate shear strain corresponding to the onset of damage. In the performed simulations we assume that the block velocity is $v=10^{-9}$ m/s and do not show the initial quasi-static loading stage. Following the onset of damage ($\xi=\xi_0$), the initial rate of damage accumulation is relatively slow. It takes more than 4000 s for damage to grow from zero to $\alpha\sim 0.3$ (red line in Fig. 10). Then, the damage growth accelerates toward its critical value, but the enhanced damping ($\eta_2=10^2$ Pa s) reduces the rate of the damage accumulation. When the distance to the critical damage value, $\Delta\alpha=\alpha_{crit}-\alpha$, is of the order of the $\beta-$value taken here to be $\beta=0.005$, the effective viscosity of the mushy region rapidly decreases (black line in Fig. 10) and enables efficient stress relaxation in the highly damage zone. The relaxation process is terminated when the elastic component of the strain is reduced to the values corresponding to $\xi=\xi_0$, when material healing starts. As shown in Fig. 10, relatively high confining pressure (100 MPa) leads to fast damage decrease (healing) and increase of the effective viscosity of the damage zone.

Two processes operate at the last stage of evolution, namely material healing due to the confining pressure and shear strain accumulation due to the ongoing plate motion. After a long-term loading stage, shear strain accumulation leads to the onset of damage growth and initiation of the next seismic cycle. A phase plane in $\alpha-\xi$ coordinate system (Fig. 11) illustrates the different stages of system evolution during a single seismic cycle. During the initial stages the evolution is quasi-static and not sensitive to the damping and width of the mushy region. During the stress relaxation stage the evolutionary path is approximately parallel to a line corresponding to $\alpha=\alpha_{crit}$ at a distance $\Delta\alpha$ that is strongly controlled by the β and η_2 values. Fig. 12 shows the effective viscosity of the mushy region as a function of $\Delta\alpha$ for different β values. The markers denote the $\Delta\alpha$ and viscosity values obtained in different numerical runs and the numbers next to the markers

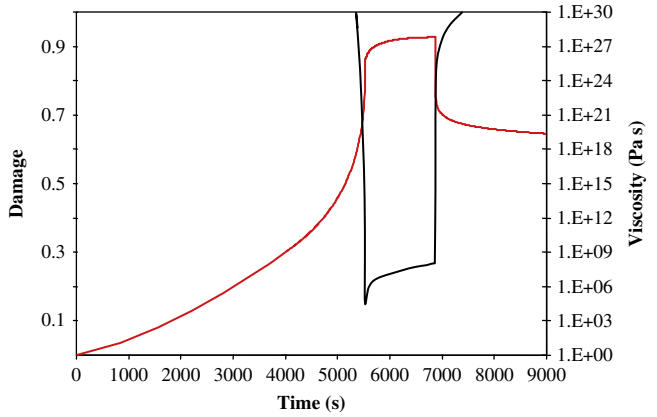

Fig. 10. Simulated damage evolution in the narrow zone (red line) and effective viscosity in the mushy region (black line). The zero time ($t=0$) corresponds to the onset of damage accumulation (the preceding long period of stress accumulation is not shown). The model parameters are: $\beta=0.005$, $\eta_2=10^2$ Pa s. The effective viscosity before $\sim$5200 s and after $\sim$7300 s is above 10^{30} Pa s. (For interpretation of the references to color in this figure legend, the reader is referred to the web version of this article.)

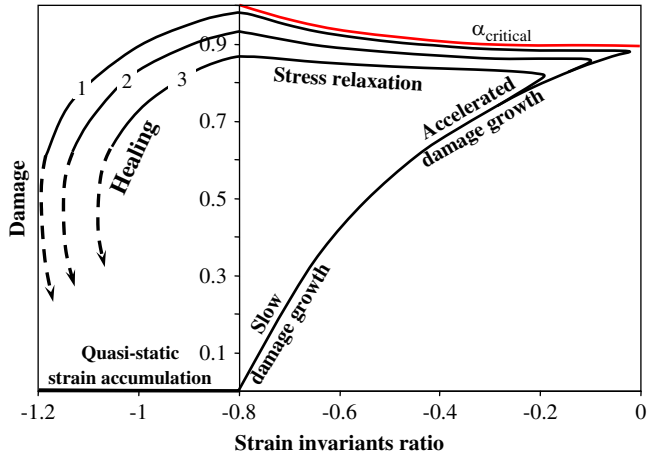

Fig. 11. Evolutionary paths of the system at different stages of deformation in the $\alpha-\xi$ phase-plane. The model parameters are: (1) $\beta=0.0001$, $\eta_2=10^4$ Pa s; (2) $\beta=0.005$, $\eta_2=10^2$ Pa s; (3) $\beta=0.001$, $\eta_2=10^2$ Pa s.

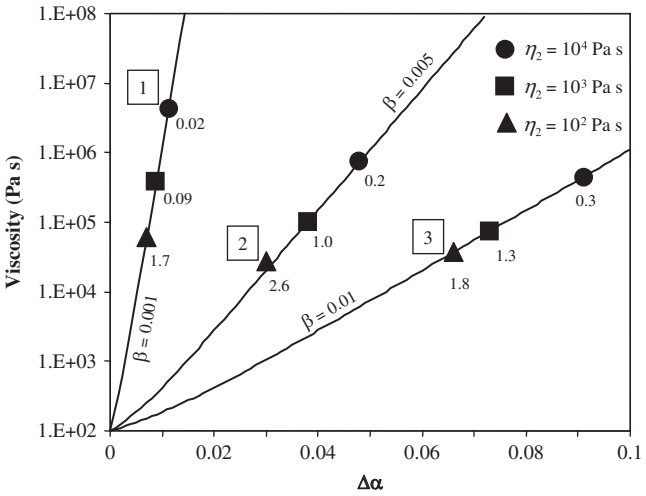

Fig. 12. Effective viscosity of the mushy region as a function of the distance to the critical damage level ($\Delta\alpha = \alpha_{crit} - \alpha$). The markers show the set of parameters used for the numerical simulations; numbers next to markers indicate maximum slip velocity obtained during the run; numbers 1, 2, 3 in quadrangles represent parameters used for the corresponding model runs of Fig. 10.

indicate the maximum slip velocity obtained in each run. Under the adopted loading conditions and model geometry, the slip velocity is above 1 m/s for effective viscosity values below 10^5 Pa s. These values of slip velocities are within the range of estimated seismic slip rates during earthquakes (e.g., Ben-Zion, 2001). The slip velocity steeply increases with the onset of the stress relaxation stage and then gradually decreases (Fig. 13). In the cases corresponding to dynamic event with slip velocity above 1 m/s (Fig. 13a), the duration of the stress relaxation stage is of the order of tens to hundred of seconds. In terms of earthquake terminology, this corresponds to the co- and early post-seismic stages. The duration of the stress relaxation stage may be as long as several hours for cases with low slip velocity (Fig. 13b). Due to high damping ($\eta_2 = 10^4$ Pa s) and narrow mushy region ($\beta = 0.001$), the effective viscosity remains relatively high (marker 1 in Fig. 12) and the relaxation process is very slow.

4. Discussion

The continuum damage mechanics employed in this study models the effects of distributed cracks in terms of a single scalar damage parameter α. Representative elementary volumes with a sufficiently large number of cracks corresponding to given values of α are assumed to be uniform and isotropic. The evolution and organization of the elementary damage zones simulated using the local version of the damage model produce macroscopic anisotropy and various patterns of large-scale fault zone structures in response to external loading (e.g., Ben-Zion et al., 1999; Lyakhovsky et al., 2001; Lyakhovsky and Ben-Zion, 2009). As shown by Lyakhovsky (2001), the process zone created by distributed damage at the tip of a mode I crack eliminates the stress singularity and provides a finite rate of quasi-static crack growth compatible with experimental observations. The model also predicts a strong asymmetry of the process zone that is generated around the tip of a pre-existing fault zone subjected to oblique loading. This asymmetry produces trajectories of the evolving newly created damage zones in out-of-plane directions that are in good agreement with the predicted directions of wing cracks under mixed mode I and mode II loading (Lyakhovsky and Ben-Zion, 2009).

It is generally agreed that analysis of distributed damage cannot be based on the classical, local constitutive models (e.g., Bazant, 1991). The non-local continuum approach, either of integral or gradient type, has generally been accepted as a proper way to avoid artificial, excessive localization and ensure mesh-independent energy dissipation (e.g., Bazant and Jirasek, 2002). A great variety of integral-type, non-local, continuum mechanics models are formulated in terms of constitutive laws involving weighted averages of a state variable over a certain neighborhood of the material point (e.g., Marotti de Sciarra, 2009 and references therein). The gradient-type models are widely used to characterize qualitative features of two-phase systems, i.e., the Ginzburg–Landau equation and the Cahn–Hilliard equation. Both these equations are based on the free energy of a continuum, which depends on the value of the order parameter (hidden state variable) at a point and also on its gradient (e.g., Gurtin, 1996).

Following the above ideas, we assume that the free energy of a damaged solid depends not only on the scalar damage parameter, α, but also on it spatial derivative, $\nabla\alpha$. The non-local, damage-gradient term leads to structural stresses in the constitutive stress–strain relations, and a damage diffusion term in the kinetic equation for damage evolution. The damage diffusion eliminates the unrealistic singular localization of the local damage model (Fig. 6), and similarly to the Ginzburg–Landau and the Cahn–Hilliard equations it leads to a diffuse interface where damage undergoes large variations. The finite width of the localization zone provides a fundamental length scale that allows numerical simulations with the model (using sufficiently small

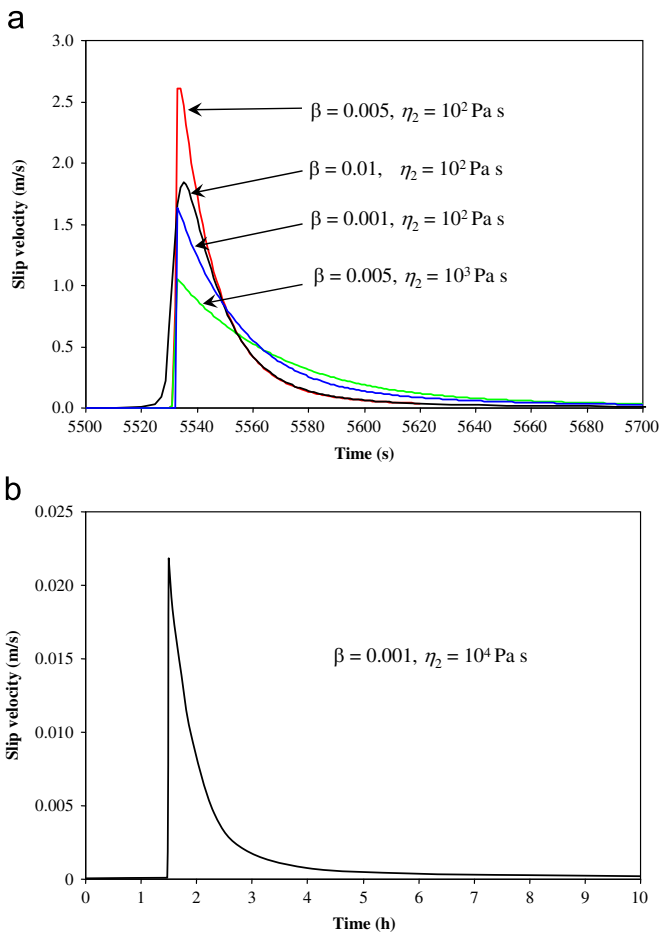

Fig. 13. Slip velocities during macroscopic instability (stress-drop) events. The maximum slip velocity may vary, depending on the β and η_2 values, from several m/s (a) typical for regular dynamic earthquakes to small fraction of m/s (b) typical for slow earthquakes.

grid size) to achieve the continuum limit. The model results predict that the width of the damage zone, w, is scaled with square root of the time-to-failure, t_f, multiplied by the damage diffusion coefficient (27). Thus, more localized damage zones are expected with same mechanical properties for short t_f, which is associated with high stress levels (18). This implies that higher shear localization is expected in deep parts of natural fault zones, in agreement with observations associated with exhumed faults (e.g., Chester et al., 1993; Sibson, 2003). Similarly, the dependency on t_f predicts higher localization for situations corresponding to lower values of the initial elastic modulus and higher values of the rate coefficient C_d of brittle damage evolution. These expectations should be tested with future laboratory experiments.

Bazant (2005) noted that nonlocal distributed damage models are capable of reproducing size effect. Our modeling results for mode-I quasi-static crack growth demonstrate that accounting for damage diffusion allows reproducing linear scaling between stress and crack length, $\sigma \propto L^{-1}$, for failures at crack initiation. In contrast to the power law scaling, $\sigma \propto L^{-1/2}$, of linear elastic fracture mechanics, the linear scaling has been experimentally observed (e.g., Bazant and Novak, 2001) and derived theoretically (Bazant, 2005) as a nonlocal generalization of the Weibull theory for failures at crack initiation. The non-dimensional damage diffusivity ratio of Eq. (30) reflects the competition between the diffusion-controlled damage delocalization in the non-local model and localization driven by external load. The value of the damage diffusivity ratio defines a transition from the linear scaling for failures at crack initiation to the power law scaling common for local damage rheology models and linear elastic fracture mechanics.

Following our previous studies (e.g., Lyakhovsky et al., 1997b; Hamiel et al., in press), the local part of the free energy includes non-analytic, second-order term, accounting for different effective elastic moduli under compression and tension, and for the increase in their difference when approaching macroscopic brittle instability. At the critical damage level the tensile modulus vanishes while the compressive modulus remains finite. A corresponding simplified 1-D stress–strain relation mimics the mechanical behavior of a cohesionless granular material where tensile stresses cannot be supported. Based on this analogy, Myasnikov and Oleinikov (1991) and Revugenko (2006) discussed a mathematical model of granular material as a limit case of media that react differently to tension and compression. The condition of macroscopic stability of solid under 3-D deformation is convexity of the elastic strain energy, which is necessary for the existence of

a unique solution for the static problem. Ben-Zion (2008) noted that the loss of convexity of the energy function at $\alpha=\alpha_{cr}$ is a hallmark of phase transitions and suggested that it signifies a transition from a highly damaged solid to a granular material. In this study we assume that similarly to the mushy region discussed in a context of the Stefan problem (e.g., Crank, 1987), near the critical state, $\alpha=\alpha_{cr}$, there exists a mixture zone with certain probability for a material point (or location in space) to be either in the solid or the granular phase. Significant reduction of the mixture zone viscosity with increasing probability of being in the granular phase provides a mechanism for fast slip accumulation and dynamic stress drop during instability event. As shown in the numerical simulations, changes of the effective viscosity of the mushy region can produce (Fig. 13) transitions between dynamic and slow slip, with low viscosities leading to fast slip events. Further theoretical and experimental investigations are needed to explore the nature of the mushy region to understand better what controls its mechanical behavior and detailed of the evolution from slow to fast slip.

Many local and non-local damage rheology models combine elasticity with Maxwell-type visco-elasticity or plasticity to account for gradual irreversible strain accumulation. These models leave out the enhanced damping of the elastic waves in highly damaged material, which can be important for some engineering and continuum mechanics applications under conditions of brittle deformation. Moreover, such models ignore important potential feedback mechanisms between changes of elastic moduli in the slipping zone and subsequent rupture behavior and radiation. For example, the reduction of elastic moduli in the shear localization zone may generate significant bimaterial interfaces, which can produce strong dynamic coupling between slip and changes of normal stress that were shown to have significant effects on the mode and properties of ruptures (e.g., Weertman, 1980; Adams, 1995; Ben-Zion 2001). The presented damage model can be used to study such feedback mechanisms and related aspects of the motion radiated to the bulk. Our damage model also includes the strain rate tensor as an additional thermodynamic state variable, leading to the Jefferys model which combines Maxwell and Kelvin–Voigt visco-elasticity (e.g., Christensen, 2003). This type of model accounts for both stress relaxation of the Maxwellian viscosity with the retardation of the Kelvin–Voigt viscosity that damps high frequency oscillations and is widely used in seismology for attenuation of seismic waves (e.g., Aki and Richards, 2002). The damage-dependent Kelvin–Voigt viscosity parameter, $\eta(\alpha)$, not only controls the quality factor in the bulk, but also significantly affects the damage growth at stages of fast damage accumulation associated with high strain rates. The performed quasi-static numerical simulations show (Fig. 4) that model solutions with or without damping are almost identical for relatively low values of damage. However, for high values of damage ($\alpha>0.7$ in the presented cases), the rates of damage growth for damped systems are capped at some levels, inversely proportional to the damping, and then strongly decreases. In the model formulation with a transition at $\alpha\to\alpha_{cr}$ to a granular phase, the low viscosity granular flow is responsible for rapid slip accumulation and transition from quasi-static to dynamic event.

Scaling analysis of the model equations can clarify the conditions that control the transition from quasi-static evolution to dynamic failure. This is done below by linearization of the relations between strain, elastic moduli and damage, as well as neglecting the irreversible strain accumulation in the force balance Eq. (40). During the acceleration stage of deformation, the rate of damage growth becomes a major factor controlling the deformational processes in the damage zone, and changes in the far field displacement may be ignored. With these assumptions the rate of motion is proportional to the rate of damage accumulation

$$\frac{du}{dt}=\frac{w}{L}\frac{u_0\alpha_{cr}}{2(\alpha_{cr}-\alpha)^2}\frac{d\alpha}{dt}. \tag{41}$$

The quasi-static approximation is valid as long as the radiation damping term in (40) is much smaller than the static strain, i.e.,

$$\delta\frac{u_0}{L}=\frac{1}{V_S}\frac{du}{dt}, \tag{42}$$

where δ is some small factor. The value of δ is scaled by the ratio between the elastic strain associated with wave propagation at the beginning of the dynamic regime ($(1/V_s)(du/dt)$) and the elastic strain at the end of the quasi-static regime (u_0/L). Brittle rocks usually fail at elastic strains of the order of $\sim10^{-2}$, while strains associated with seismic waves are at least three orders of magnitude less, i.e., $\delta<10^{-3}$. Condition (42) together with Eq. (41) can be used to define "dynamic damage", α_d, at the transition from quasi-static to dynamic regime

$$\alpha_d=\alpha_{cr}-\sqrt{\frac{w\alpha_{cr}}{2\delta V_s}\frac{d\alpha}{dt}}. \tag{43}$$

A similar expression in the form $\alpha_d=\alpha_{cr}-\sqrt{\tau_d\dot{\alpha}}$ was adopted by Lyakhovsky (2001) to account for dynamic weakening in quasi-static modeling and simulate a transition from quasi-static to dynamic fracturing. Previous derivations based on general dynamic stability analysis of the damaged material (Ben-Zion and Lyakhovsky, 2006) provided the square root correction to the critical α-value, but did not connect the dynamic weakening parameter, τ_d, with specific physical properties. Using $\alpha_{cr}=1$ in (41), the above derivation provides the following explicit connection between different physical parameters of the model

$$\tau_d=\frac{w}{2\delta V_s}. \tag{44}$$

Ben-Zion and Lyakhovsky (2006) constrained the value of τ_d for situations corresponding to natural fault zones, by requiring that simulated aftershock sequences with the local damage rheology model are consistent with the empirical Bath law (the magnitude of largest aftershock is ~ 1 unit less than that of the mainshock). Simulations with width of damage zone $w=500$ m led to $\tau_d=3\times 10^2-3\times 10^4$ s. This range is comparable to what is predicted by (44) with $V_s\sim 3$ km/s, $w=500$ m, and $\delta=5\times 10^{-4}-5\times 10^{-6}$. Hence, relation (44) with the above estimated δ-factor provides a physical basis for scaling the dynamic damage-weakening parameter τ_d to other model parameters. The results imply that the slow quasi-static deformation phase preceding the dynamic failure can be successfully simulated with the local damage version of the model that employs the dynamic damage variable (43). However, a quantitative description of the transition to the dynamic regime and detailed analysis of associated deformation features (localization width, slip velocity, etc.) require the entire formulation presented in this study. A more complete analysis of the deformation processes preceding and following the occurrence of brittle instabilities (loss of convexity in the discussed model) will require additional details on the functional forms associated with the transitions between highly damaged solid and granular material. This will be the subject of a follow up work.

Acknowledgments

We thank J. Fineberg and A. Ilchev for discussions. The paper benefitted from constructive comments by two anonymous reviewers and Editor Huajian Gao. The authors acknowledge support by the US–Israel Binational Science Foundation (Grant 2008248) and the National Science Foundation (Grant EAR-0908903).

Appendix A. Thermodynamic formulation

The total energy of a solid with a unit mass includes internal and kinetic components:

$$E=E_k+U. \tag{a1}$$

The specific kinetic energy of the solid is $E_k=v_iv_i/2$ with v_i being velocity, while the internal energy is expressed through the free energy F, temperature T, and entropy S as $U=F+TS$. The energy balance equation dictates that the change in the energy of a system is equal to the divergence of the heat flux $J_i^{(q)}$ and total external work W

$$\frac{dE}{dt}=\frac{dE_k}{dt}+\frac{d}{dt}(F+TS)=-\nabla_i J_i^{(q)}+W. \tag{a2}$$

The entropy balance equation includes entropy flux $J_i^{(s)}$ and non-negative local entropy production Γ

$$\frac{dS}{dt}=-\nabla_i J_i^{(s)}+\Gamma, \quad \Gamma\geq 0. \tag{a3}$$

The non-negative local entropy production results from all the dissipative irreversible processes in the solid including internal friction and damage evolution. From (a2), the change in the free energy can be expressed as

$$dF=-SdT+\frac{\partial F}{\partial \varepsilon_{ij}}d\varepsilon_{ij}+\frac{\partial F}{\partial e_{ij}}de_{ij}+\frac{\partial F}{\partial \alpha}d\alpha+\frac{\partial F}{\partial(\nabla_i\alpha)}d(\nabla_i\alpha). \tag{a4}$$

In a system with internal motions, the time derivative is given by $d/dt=\partial/\partial t+v_i\nabla_i$. Similarly,

$$\nabla_i\left(\frac{d\alpha}{dt}\right)=\nabla_i\left(\frac{\partial\alpha}{\partial t}+v_k\nabla_k\alpha\right)=\frac{d(\nabla_i\alpha)}{dt}+e_{ik}\nabla_k\alpha. \tag{a5}$$

From (a5), the time derivative of the last term in (a4) can be written as

$$\frac{\partial F}{\partial(\nabla_i\alpha)}\frac{d(\nabla_i\alpha)}{dt}=-\left[\nabla_i\left(\frac{\partial F}{\partial(\nabla_i\alpha)}\right)\frac{d\alpha}{dt}+e_{ik}\frac{\partial F}{\partial(\nabla_i\alpha)}\nabla_k\alpha\right]+\nabla_i\left(\frac{\partial F}{\partial(\nabla_i\alpha)}\frac{d\alpha}{dt}\right). \tag{a6}$$

The local entropy production may be represented as

$$\Gamma-\nabla_i\left(J_i^{(s)}-\frac{J_i^{(q)}}{T}-\frac{1}{T}\frac{\partial F}{\partial(\nabla_i\alpha)}\frac{d\alpha}{dt}\right)=\Gamma_M+\Gamma_H+\Gamma_V+\Gamma_D. \tag{a7}$$

The terms on the right side of (a6) are associated with the following energy components:
Mechanical work

$$\Gamma_M=-\frac{1}{T}\left[v_i\frac{dv_i}{dt}+\left(\frac{\partial F}{\partial\varepsilon_{ij}}-\frac{\partial F}{\partial(\nabla_i\alpha)}\nabla_j\alpha\right)e_{ij}-W\right], \tag{a8}$$

Heat transport

$$\Gamma_H=-\frac{1}{T^2}\left(J_i^{(q)}+\frac{\partial F}{\partial(\nabla_i\alpha)}\frac{d\alpha}{dt}\right)\nabla_i T, \tag{a9}$$

Viscous deformation

$$\Gamma_V = \frac{1}{T}\left(\frac{\partial F}{\partial \varepsilon_{ij}}\frac{dg_{ij}^{(0)}}{dt} - \frac{\partial F}{\partial e_{ij}}\frac{de_{ij}}{dt}\right), \tag{a10}$$

and damage evolution

$$\Gamma_D = -\frac{1}{T}\left(\frac{\partial F}{\partial \alpha} - \nabla_i \frac{\partial F}{\partial(\nabla_i \alpha)}\right)\frac{d\alpha}{dt}. \tag{a11}$$

Following the literature of non-equilibrium thermodynamic (e.g., de Groot and Mazur, 1962), the divergence term on the left side of (a7) is eliminated by defining the entropy flux as

$$J_i^{(s)} = \frac{J_i^{(q)}}{T} + \frac{1}{T}\frac{\partial F}{\partial(\nabla_i \alpha)}\frac{d\alpha}{dt}. \tag{a12}$$

In addition to the usual relation $J_i^{(s)} = J_i^{(q)}/T$ of local models, Eq. (a12) includes a second entropy flux component that is associated with damage evolution in the non-local formulation.

The equation of motion of a continuum is given by the standard relation

$$\rho\frac{dv_i}{dt} = \frac{\partial \sigma_{ij}}{\partial x_j} + f_i, \tag{a13}$$

where f_i is the body force. The model formulation should satisfy conservation of mechanical energy ($\Gamma_M = 0$) if all the dissipative processes in the system are frozen. This condition leads to the definition of the stress tensor

$$\sigma_{ij} = \rho\left[\frac{\partial F}{\partial \varepsilon_{ij}} - \frac{1}{2}\left(\frac{\partial F}{\partial(\nabla_i \alpha)}\nabla_j \alpha + \frac{\partial F}{\partial(\nabla_j \alpha)}\nabla_i \alpha\right)\right]. \tag{a14}$$

Since the entropy flux Γ_M in (a8) includes, in addition to the usual term $\partial F/\partial \varepsilon_{ij}$ (e.g., Malvern, 1969), terms associated with $\nabla\alpha$, there are related "structural stresses" in the constitutive relations (a14). These stresses are associated with heterogeneous damage distribution and can be important in zones with high $\nabla\alpha$ values.

Appendix B. Wave attenuation in damaged rocks

Experimental measurements of wave attenuation in various rocks have been studied extensively (e.g., Born, 1941; Nur and Simmons, 1969; Johnston et al., 1978; Winkler and Nur, 1982; Liu and Ahrens, 1997; Van Den Abeele et al., 2000; Wulff et al., 1999; Ai and Ahrens, 2007). Several theoretical models were developed to relate wave attenuation to crack density of dry and saturated cracked media (e.g., Walsh 1966,; Mavko et al., 1979; Johnston et al., 1978; Chatterjee et al., 1980; Hudson, 1981; Aki, 1982; Caleap et al., 2009). The commonly used attenuation mechanisms include friction, fluid flow and scattering. Some authors consider friction on thin cracks and grain boundaries as a dominant attenuation mechanism for consolidated rocks; others attribute attenuation primarily to energy loss related to fluid flow. Several studies relate the dispersion and attenuation of seismic waves to scattering by heterogeneities embedded in the Earth's crust. Because all theoretical models connect wave attenuation with the existence of cracks and other types of defects, the

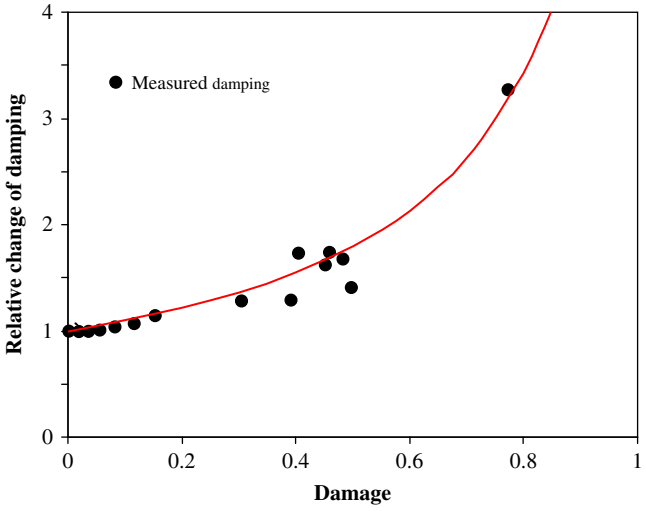

Fig. b1. Measured attenuation for *P* waves in synthetic brittle material versus damage (after Van Den Abeele et al., 2000). The line shows a fit to the data using Eq. (b2).

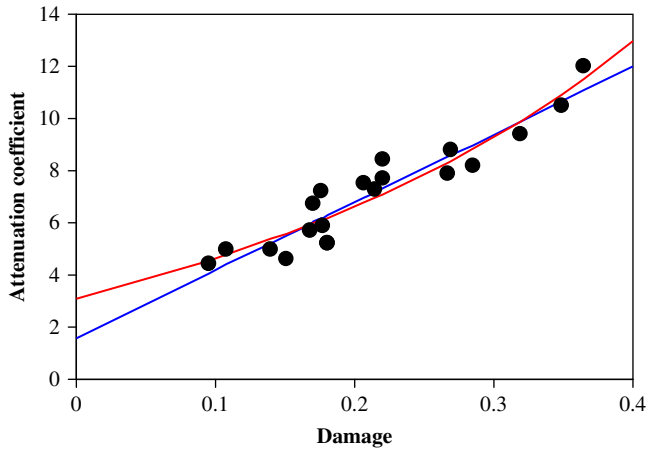

Fig. b2. Measured attenuation for *P* waves in gabbroic samples versus damage (after Liu and Ahrens, 1997). The blue curve shows the linear fit suggested by the authors. The red line provides a slightly better fit using Eq. (b2). (For interpretation of the references to color in this figure legend, the reader is referred to the web version of this article.)

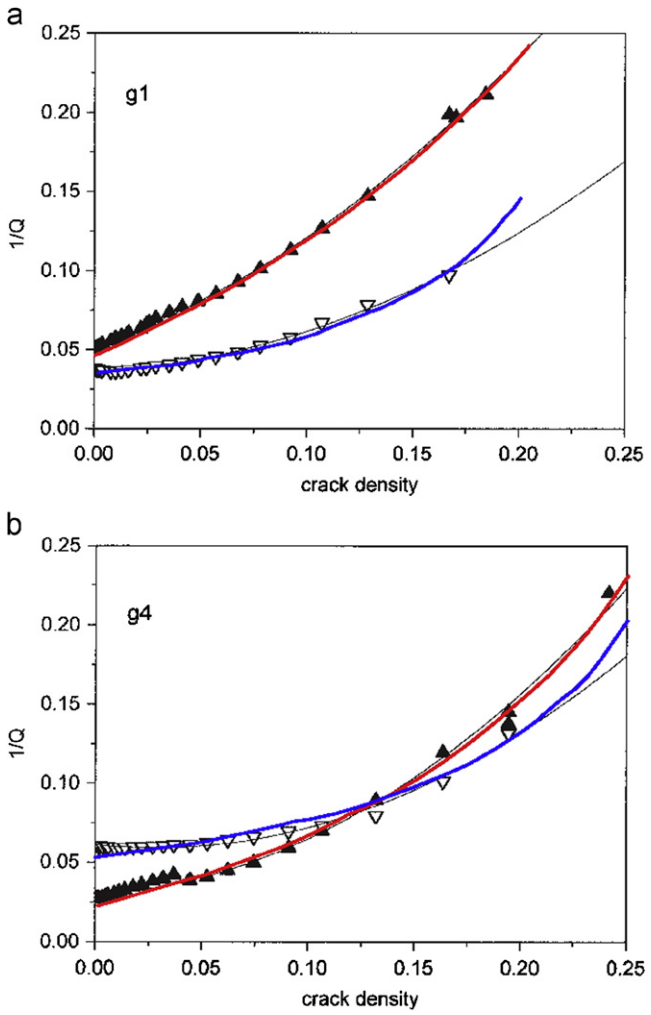

Fig. b3. Measured attenuation for *P* (closed symbols) and *S* waves (open symbols) versus damage for granite samples (after Wulff et al., 1999). The black curves show the quadratic fit suggested by the authors. The colored lines represent fitting with Eq. (b2). (For interpretation of the references to color in this figure legend, the reader is referred to the web version of this article.)

relationship between the attenuation coefficient and rock damage is important for understanding wave propagation in rocks.

Theoretical models considering effective elastic properties of rocks with randomly distributed or oriented micro-cracks predict linear increase of the attenuation coefficient with micro-crack density. Liu and Ahrens (1997) and others used in laboratory studies of acoustic rock properties a damage parameter, D, defined as

$$D = 1 - \left(\frac{V}{V_0}\right)^2, \tag{b1}$$

where V is the velocity of the cracked rock and V_0 is the intrinsic rock velocity. Neglecting pressure-induced density change, the damage is equivalent to the reduction of the elastic modulus divided by the elastic modulus of the undamaged rock, and is directly connected to the crack density (e.g., O'Connel and Budiansky, 1974). Figs. b1–b3 present experimentally measured attenuation coefficient as function of material damage, along with several line fits to the data.

Most of the experimental results (Figs. b1, b3) suggest stronger increase of the attenuation coefficient with rock damage than a linear trend. The only experimental results (Fig. b1) with highly damaged material suggest steep increase of the attenuation prior to the material failure. Following this observation we speculate that seismic waves are over-damped in highly damaged rocks. Beyond some damage level the rocks cannot support load and hence mechanical oscillations cannot propagate. This means that the attenuation coefficient $\zeta(D)$ should approach infinity toward the failure and may be approximated as

$$\zeta(D) = \zeta_1 + \frac{\zeta_2}{D_{cr} - D}. \tag{b2}$$

This is the simplest mathematical expression that includes only two fitting parameters, ζ_1, ζ_2 and a critical damage value, D_{cr}, at failure. Figs. b1–b3 show fits to experimental data with this equation. The data of Fig. b1 are strongly non-linear and can be fitted well by Eq. (b2). The other experimental data were measured in relatively narrow ranges of damage values and the fit with Eq. (b2) is of similar quality to fits using linear (Fig. b2) or quadratic (Fig. b3) relations suggested by others. At the very least, the experimental data are not inconsistent with the proposed relation (b2) between the attenuation coefficient $\zeta(D)$ and damage. More general formulation should probably also account for a frequency-dependent damping by including frequency in the functional relation (b2) for the attenuation coefficient.

References

Adams, G.G., 1995. Self-excited oscillations of two elastic half-spaces sliding with constant coefficient of friction. J. Appl. Mech 62, 867–872.

Agnon, A., Lyakhovsky, V., 1995. Damage distribution and localization during dyke intrusion. In: Baer, G., Heimann, A. (Eds.), The Physics and Chemistry of Dykes. Balkema, Rotterdam, pp. 65–78.

Ai, H.A., Ahrens, T.J., 2007. Effects of shock-induced cracks on the ultrasonic velocity and attenuation in granite. J. Geophys., Res. 112, B01201, doi:10.1029/2006JB004353.

Aki, K., 1982. Scattering and attenuation. Bull. Seism. Soc. Am 72, S319–S330.

Aki, K., Richards, P.G, 2002. Quantitative Seismology, 2nd ed. University Science Books.

Allix, O., Hild, F., 2002. Continuum Damage Mechanics of Materials and Structures. Elsevier (396 pp).

Ashby, M.F., Sammis, C.G., 1990. The damage mechanics of brittle solids in compression. Pure Appl. Geophys. 133, 489–521.

Barenblatt, G.I., 1996. Scaling, Self-similarity, and Intermediate Asymptotics. Cambridge Univ. Press.

Bazant, Z.P., Cedolin, L., 1991. Stability of Structures. Elastic, Inelastic, Fracture and Damage Theories. Oxford University Press, pp. 984.

Bazant, Z.P., Jirasek, M., 2002. Nonlocal integral formulations of plasticity and damage: survey of progress. J. Engineering Mech. 128, 1119–1149.

Bazant, Z.P., Novak, D., 2001. Nonlocal theory and size effect in failure at fracture initiation. In: de Borst, R., Mazars, J., Pijaudier-Cabot, G., van Mier, J.G.M. (Eds.), Fracture Mechanics of Concrete Structures, pp. 659–664.

Bazant, Z.P., 1991. Why continuum damage is nonlocal: Micromechanics arguments. J. Eng. Mech., ASCE 117 (5), 1070–1087.

Bazant, Z.P., 2005. Scaling of Structural Strength. Elsevier.

Ben-Zion, Y., Lyakhovsky, V., 2006. Analysis of aftershocks in a lithospheric model with seismogenic zone governed by damage rheology. Geophys. J. Int. 165, 197210.

Ben-Zion, Y., Rice, J.R., 1995. Slip patterns and earthquake populations along different classes of faults in elastic solids. J. Geophys. Res. 100, 12959–12983.

Ben-Zion, Y., 2001. Dynamic rupture in recent models of earthquake faults. J. Mech. Phys. Solids 49, 2209–2244.

Ben-Zion, Y., 2008. Collective behavior of earthquakes and faults: continuum-discrete transitions, evolutionary changes and corresponding dynamic regimes. Rev. Geophys. 46, RG4006, doi:10.1029/2008RG000260.

Ben-Zion, Y., Dahmen, K.A., Uhl, J.T. A unifying phase diagram for the dynamics of sheared solids and granular materials. Pure Appl. Geophys., in press. doi:10.1007/s00024-011-0273-7.

Ben-Zion, Y., Dahmen, K., Lyakhovsky, V., Ertas, D., Agnon, A., 1999. Self-driven mode switching of earthquake activity on a fault system. Earth Planet. Sci. Lett. 172, 11–21.

Ben-Zion, Y., Lyakhovsky, V., 2002. Accelerating seismic release and related aspects of seismicity patterns on earthquake faults. Pure Appl. Geophys. 159, 2385–2412.

Berdichevsky, V.L., 2009. Variational Principles of Continuum Mechanics. Springer Verlag.

Biot, M.A., 1955. Variational principles in irreversible thermodynamics with application to viscoelasticity. Phys. Rev. 97, 1463–1469.

Born, W.T., 1941. The attenuation constant of Earth materials. Geophysics 6, 132–148.

Briscoe, C., Song, C., Wang, P., Makse, H.A., 2008. Entropy of jammed matter. Phys Rev. Lett. 101, 188001(4).

Budiansky, B., O'Connell, R.J., 1976. Elastic moduli of a cracked solid. Int. J. Solids Struct. 12, 81–97.

Caleap, M., Aristegui, C., Angel, Y.C., 2009. Effect of crack opening and orientation on dispersion and attenuation of antiplane coherent wave. Geophys. J. Int. 177, 1151–1165.

Chandelier, R., Dauchot, O., 2010. Journey of an intruder through the fluidization and jamming transitions of a dense granular media. Phys. Review E 81, 011304(12).

Chapman, S., Cowling, T.G., 1964. The Mathematical Theory of Nonuniform Gases, 2nd edn. Cambridge Univ. Press, Cambridge.

Charles, R.J., 1958. Static fatigue of glass. J. Appl. Phys. 29, 1549–1560.

Chatterjee, A.K., Mal, A.K., Knopoff, L., Hudson, J.A., 1980. Attenuation of elastic waves in a cracked, fluid-saturated solid. Mathematical Proceedings of the Cambridge Philosophical Society 88, 547–561 (Cambridge University Press).
Chester, F.M., Evans, J.P., Biegel, R.L., 1993. Internal structure and weakening mechanisms of the San Andreas fault. J. Geophys. Res. 98, 771–786.
Christensen, R.M., 2003. In: Theory of Viscoelasticity. Dover Publications, Mineola, New York.
Coniglio, A., de Candia, A., Fierro, A., Nicodemi, M., Pica Ciamarra, M., Tarzia, M., 2004. On Edwards' theory of powders. Physica A 339, 1–6.
Crank, J., 1987. Free and Moving Boundary Problems. Oxford Univ. Press, New York (424 pp.).
D'Anna, G., Gremaud, G., 2001. The jamming route to the glass state in weakly perturbed granular media. Nature 413, 407–409.
de Groot, S.R., Mazur, P., 1962. Nonequilibrium Thermodynamics. North-Holland Publishing Co., Amsterdam (510 pp.).
Deshpande, V.S., Evans, A.G., 2008. Inelastic deformation and energy dissipation in ceramics: a mechanism-based constitutive model. J. Mech. Phys. Solids 56, 3077–3100.
Dieterich, J.H., 1972. Time-dependent friction in rocks. J. Geophys. Res. 77, 3690–3697.
Dieterich, J.H., 1979. Modeling of rock friction 1. Experimental results and constitutive equations. J. Geophys. Res. 84, 2161–2168.
Drucker, D.C., 1949. Some implications of work-hardening and ideal plasticity. Quart. Appl. Math. 7, 411–418.
Edwards, S.F., Oakeshott, R.B.S., 1989. Theory of powders. Physica A 157, 1080–1090.
Edwards, S.F., 1990. The rheology of powders. Rheol. Acta 29, 493–499.
Edwards, S.F., 2005. The full canonical ensemble of a granular system. Physica A 353, 114–118.
Ekland, I., Temam, R., 1976. Convex Analysis and Variational Problems. Elsevier.
Eringen, A.C., 1966. A unified theory of thermomechanical materials. Int. J. Eng. Sci. 4, 179–202.
Fitts, D.D., 1962. Nonequilibrium Thermodynamics. McGraw-Hill Book Company, New York (173 pp.).
Gurtin, M.E., 1996. Generalized Ginzburg–Landau and Cahn–Hilliard equations based on a microforce balance. Physica D 92, 178–192.
Hamiel, Y., Liu, Y., Lyakhovsky, V., Ben-Zion., Y., Lockner, D., 2004. A visco-elastic damage model with applications to stable and unstable fracturing. J. Geophys. Int. 159, Î11.
Hamiel, Y., Lyakhovsky, V., Agnon, A., 2005. Rock dilation, nonlinear deformation, and pore pressure change under shear. Earth Planet. Sci. Lett. 237, 57Ï589.
Hamiel, Y., Lyakhovsky, V., Ben-Zion, Y. The elastic strain energy of damaged solids with applications to nonlinear deformation of crystalline rocks. Pure Appl. Geophys., in press. doi:10.1007/s00024-011-0265-7.
Hamiel, Y., Lyakhovsky, V., Stanchits, S., Dresen, G., Ben-Zion, Y., 2009. Brittle deformation and damage-induced seismic wave anisotropy in rocks. Geophys. J. Int. 178, 901–909.
Heermance, R., Shipton, Z.K., Evans, J.P., 2003. Fault structure control on fault slip and ground motion during the 1999 rupture of the Chelungpu fault, Taiwan. Bull. Seis. Soc. Am. 93, 1034–1050.
Hill, R., 1998. The Mathematical Theory of Plasticity. Oxford University Press 368 pp.
Hudson, J.A., 1981. Wave speed and attenuation of elastic waves in material containing cracks. Geophys. J. R. Astr. Soc. 64, 133–150.
Jaeger, H.M., Nagel, S.R., Behringer, R.P., 1996. Granular solids, liquids, and gases. Rev. Mod. Phys. 68, 1259–1273.
Johnston, D.H., Toksoz, M.N., Timur, A., 1978. Attenuation of seismic waves in dry and saturated rocks: theoretical models and mechanisms. J. Geophys., Res., 691–711.
Kachanov, L.M., 1986. Introduction to Continuum Damage Mechanics. Martinus Nijhoff Publishers (135 pp.).
Kohlstedt, D.L., Evans, B., Mackwell, S.J., 1995. Strength of the lithosphere: constraints imposed by laboratory experiments. J. Geophys. Res. 100, 17587–17602.
Krajcinovic, D., 1996. Damage Mechanics. Elsevier, Amsterdam.
Kroner, E., 1968. Elasticity theory of materials with long-range cohesive force. Int. J. Solids Struct. 3, 731–742.
Landau, L.D., Lifshitz, E.M., 1980. 3rd editionStatistical Physics, Course of Theoretical Physics, vol. 5. Pergamon Press, Oxford (387 pp).
Lemaitre, J., 1996. A Course on Damage Mechanics. Springer Verlag, Berlin (228 pp).
Liu, A.J., Nagel, S.R. (Eds.), 2001. Jamming and Rheology: Constrained Dynamics on Microscopic and Macroscopic Scales. Taylor and Francis, London.
Liu, A.J., Nagel, S.R., 1998. Jamming is not just cool any more. Nature 396, 21–22.
Liu, C., Ahrens, T.J., 1997. Stress wave attenuation in shock-damaged rock. J. Geophys. Res. 102, 5243–5250.
Lockner, D.A., Byerlee, J.D., Kuksenko, V., Ponomarev, A., Sidorin, A., 1992. Observations of quasi-static fault growth from acoustic emissions. In: Evans, B., Wong, T.-f. (Eds.), Fault Mechanics and Transport Properties of Rocks, International Geophysics Series, vol. 51. Academic Press, San Diego, CA, pp. 3–31.
Lyakhovsky, V., 2001. Scaling of fracture length and distributed damage. Geophys. J. Int. 144, 114–122.
Lyakhovsky, V., Ben-Zion, Y., 2008. Scaling relations of earthquakes and aseismic deformation in a damage rheology model. Geophys. J. Int. 172, 651–662.
Lyakhovsky, V., Ben-Zion, Y., 2009. Evolving geometrical and material properties of fault zones in a damage rheology model. Geochem. Geophys. Geosyst. 10, Q11011. doi:10.1029/2009GC002543.
Lyakhovsky, V., Myasnikov, V.P., 1984. On the behavior of elastic cracked solid, Phys. Solid Earth 10, 71–75.
Lyakhovsky, V., Myasnikov, V.P., 1985. On the behavior of visco-elastic cracked solid. Phys. Solid Earth 4, 28–35.
Lyakhovsky, V., Ben-Zion, Y., Agnon, A., 1997a. Distributed damage, faulting, and friction. J. Geophys. Res. 102, 27635–27649.
Lyakhovsky, V., Reches, Z., Weinberger, R., Scott, T.E., 1997b. Non-linear elastic behavior of damaged rocks. Geophys. J. Int. 130, 157–166.
Lyakhovsky, V., Ben-Zion, Y., Agnon, A., 2005. A viscoelastic damage rheology and rate- and state-dependent friction. Geophys. J. Int. 161, 179–190.
Lyakhovsky, V., Hamiel, Y., Ampuero, P., Ben-Zion, Y., 2009. Nonlinear damage rheology and wave resonance in rocks. Geophys. J. Int. 178, 910–920.
Makse, A.H., Kurchan, J., 2002. Testing the thermodynamic approach to granular matter with a numerical model of a decisive experiment. Nature 415, 614–617.
Makse, H.A., Brujic, J., Edwards, S.F., 2004. Statistical mechanics of jammed matter. In: Hinrichsen, H., Wolf, D.E. (Eds.), The Physics of Granular Media. Wiley-VCH Verlag, Weinheim, pp. 45–85.
Malvern, L.E., 1969. Introduction to the Mechanics of a Continuum Medium. Prentice-Hall, Inc., New Jersey (713 pp.).
Marone, C., 1998. Laboratory-derived friction laws and their application to seismic faulting. Annu. Rev. Earth Planet. Sci. 26, 643–649.
Marotti de Sciarra, F.M., 2009. A nonlocal model with strain-based damage. Int. J. Solids Struct. 46, 4,107–4,122.
Martyushev, L., Seleznev, V., 2006. Maximum entropy production principle in physics, chemistry and biology. Phys. Rep. 426, 1–45.
Mavko, G., Kjartansson, E., Winkler, K., 1979. Seismic wave attenuation in rocks. Rev. Geophys. Space Phys. 17, 1155–1164.
McNamura, S., Richard, P., de Richter, S.K., Le Caer, G., Delannay, R., 2009. Measurements of granular entropy. Phys. Rev. E 80, 031301(14).
Mehta, A., Edwards, S.F., 1989. Statistical mechanics of powder mixtures. Physica A 157, 1091–1100.
Metzger, P.T., Donahue, C.M., 2005. Elegance of disordered granular packings: a validation of Edwards hypothesis. Phys. Rev. Lett. 94, 148001(4).
Myasnikov, V., Lyakhovsky, V., Podladchikov, Yu, 1990. Non-local model of strain-dependent visco-elastic media. Doklady Ac. Sci. USSR 312, 302–305.
Myasnikov, V.P., Oleinikov, A.I., 1991. Deformation model of a perfectly free-flowing granular medium. Soviet Phys. Doklady 36, 51–53.
Nemat-Nasser, S., Hori, M., 1999. In: Micromechanics: Overall Properties of Heterogeneous Solids 2nd ed. Elsevier Science Publishers (810 pp.).
Newman, W.I., Phoenix, S.L., 2001. Time-dependent fiber bundles with local load sharing. Phys. Rev. E 63, 2 (Art. No. 021507).
Nur, A., Simmons, G., 1969. The effect of viscosity of a fluid phase on velocity in low porosity rocks. Earth Planet. Sci. Lett 7, 99–108.
O'Connell, R.J., Budiansky, B., 1974. Seismic wave velocities in dry and saturated cracked solid. J. Geophys. Res. 79, 5412–5426.
Onsager, L., 1931. Reciprocal relations in irreversible processes. Phys. Rev 37, 405–416.
Paris, P.C., Erdogan, F., 1963. A critical analysis of crack propagation laws. J. Basic Eng., ASME Trans., Ser. D 85, 528–534.
Paterson, M.S., Wong, T.-f, 2005. In: Experimental Rock Deformation—The Brittle Field 2nd ed. Springer-Verlag, Berlin (347 pp.).

Prigogine, I., 1955. Introduction to Thermodynamics of Irreversible Processes. Springfield, Illinois.
Rabotnov, Y.N., 1988. Mechanics of deformable solids. Science, 712 (Moscow).
Rao, K.K., Nott, P.R., 2008. An Introduction to Granular Flow. Cambridge Univ. Press, Cambridge (490 pp.).
Regenauer-Lieb, K., Yuen, D.A., 2003. Modeling shear zones in geological and planetary sciences: solid-and fluid–thermal–mechanical approaches. Earth-Sci. Rev. 63, 295–349.
Revuzhenko, A.F., 2006. Mechanics of Granular Media. Springer, Berlin (308 pp.).
Rice, J.R., 1993. Spatio-temporal complexity of slip on a fault. J. Geophys. Res. 98, 9885–9907.
Rice, J.R., Ben-Zion, Y., 1996. Slip complexity in earthquake fault models. Proc. Natl. Acad. Sci. USA 93, 3811–3818.
Rockwell, T.K., Ben-Zion, Y., 2007. High localization of primary slip zones in large earthquakes from paleoseismic trenches: observations and implications for earthquake physics. J. Geophys. Res. 112, B10304, doi:10.1029/2006JB004764.
Rudnicki, J.W., Rice, J.R., 1975. Conditions for the localization of deformation in pressure-sensitive, dilatant materials. J. Mech. Phys. Solids 23, 371–394.
Savage, S.B., 1998. Analyses of slow high-concentration flows of granular materials. J. Fluid Mech. 377, 1–26.
Schreyer, H.L., Neilsen, M.K., 1996a. Analytical and numerical tests for loss of material stability. Int. J. Num. Methods Eng. 39, 1721–1736.
Schreyer, H.L., Neilsen, M.K., 1996b. Discontinuous bifurcation states for associated smooth plasticity and damage with isotropic elasticity. Int. J. Solids Struct. 33, 3239–3256.
Schroter, M., Goldman, D.I., Swinney, H.L., 2005. Stationary state fluctuations in a granular medium. Phys. Rev. E 71, 030301(4).
Sedov, L.I., 1968. Variational methods of constructing models of continuous media. In: Parkus, H., Sedov, L.I. (Eds.), Irreversible Aspects of Continuum Mechanics and Transfer of physical characteristics in Moving Fluids. Springer-Verlag, Wien/New York, pp. 17–40.
Sibson, R.H., 2003. Thickness of the seismic slip zone. Bull. Seis. Soc. Am. 93, 1169–1178.
Song, C., Wang, P., Makse, H.A., 2008. A phase diagram for jammed matter. Nature 453, 629–632.
Trappe, V., Prasad, V., Cipelletti, L., Segre, P.N., Weitz, D.A., 2001. Jamming phase diagram for attractive particles. Nature 411, 722–775.
Truesdell, C., Noll, W., 2004. In: Antman, S.S. (Ed.), The Non-Linear Field Theories of Mechanics 3rd ed. Springer-Verlag, Berlin, pp. 627.
Turcotte, D.L., Newman, W.I., Shcherbakov, R., 2003. Micro and macroscopic models of rock fracture. Geophys. J. Int. 152, 718–728.
van den Abeele, K.E.-A., Carmeliet, J., TenCate, J.A., Johnson, P.A., 2000. Nonlinear elastic wave spectroscopy (NEWS) techniques to discern material damage. Part II: single mode nonlinear resonance acoustic spectroscopy. Res. Nondestr. Eval. 12/1, 31–42.
Walsh, J.B., 1966. Seismic wave attenuation in rock due to friction. J. Geophys. Res. 71, 2591–2599.
Weertman, J., 1978. Creep laws for the mantle of the Earth. Philos. Trans. R. Soc. London A 288, 9–26.
Weertman, J., 1980. Unstable slippage across a fault that separates elastic media of different elastic constants. J. Geophys. Res. 85, 1455–1461.
Winkler, K.W., Nur, A., 1982. Seismic attenuation: effects of pore fluids and frictional sliding. Geophysics 47, 1–15.
Wulff, A.-M., Hashida, T., Watanabe, K., Takahashi, H., 1999. Attenuation behaviour of tuffaceous sandstone and granite during microfracturing. Geophys. J. Int. 139, 395–409.
Yukutake, H., 1989. Fracturing process of granite inferred from measurements of spatial and temporal variations in velocity during triaxial deformation. J. Geophys. Res. 94, 15639–15651.
Zang, A., Wagner, F., Stanchits, S., Janssen, C., Dresen, G., 2000. Fracture process zone in granite. J. Geophys. Res. 105, 23651–23661.
Ziegler, H., 1983. In: An Introducton to Thermomechanics 2nd edn North-Holland Publishing Company, Amsterdam (358 pp.).
Zietlow, W.K., Labuz, J.F., 1998. Measurement of the intrinistic process zone in rock using acoustic emission. Int. J. Rock Mech. Min. Sci. 35, 291–299.